Title
Aggregation and Rheology of Concentrated Mineral Suspensions

Author
Timmons, Jason Tyler

Publication Date
2019

Peer reviewed|Thesis/dissertation

UNIVERSITY OF CALIFORNIA

Los Angeles

Aggregation and Rheology of Concentrated Mineral Suspensions

A thesis submitted in partial satisfaction
of the requirements for the degree Master of Science
in Materials Science and Engineering

by

Jason Tyler Timmons

2019

ABSTRACT OF THE THESIS

Aggregation and Rheology
of Concentrated Mineral Suspensions

by
Jason Tyler Timmons

Master of Science in Materials Science and Engineering
University of California, Los Angeles, 2019
Professor Gaurav Sant, Chair

Suspension rheology plays a significant role in a wide variety of industries and applications: mineral processing, construction materials, paints and coatings, and drug delivery, for example. Although advances in the science of suspension rheology have been made consistently for centuries, many systems exist for which their rheological behavior is inadequately described by existing generalized models. Two systems are considered which display unexpected rheological behavior: the first is a model system of glass spheres in a polymeric fluid, and the second is a real system of irregularly shaped portlandite particles in aqueous suspension with added polymer dispersants. A thorough examination of the aggregation behavior of both systems, through analysis of rheometric experiments and secondary techniques such as light scattering, reveals details of interparticle interactions and aggregation/dispersion mechanisms which may be overlooked by simplified models. These findings advance the ability to tailor suspensions with anomalous behavior to desired rheological properties.

The thesis of Jason Tyler Timmons is approved.

Jaime Marian

Mathieu Bauchy

Gaurav Sant, Committee Chair

University of California, Los Angeles

2019

TABLE OF CONTENTS

LIST OF FIGURES

LIST OF TABLES

ACKNOWLEDGEMENTS

Chapter 2 is a version of: Timmons, J., Falzone, G., Balonis, M., Bauchy, M. and Sant, G., 2018. Anomalous variations in the viscous activation energy of suspensions induced by fractal structuring. Journal of colloid and interface science, 530, pp.603-609, https://doi.org/10.1016/j.jcis.2018.07.008. The authors acknowledge financial support for this research provisioned by the National Science Foundation (CMMI: 1401533, 1562066, CAREER Award: 1253269), and University of California, Los Angeles (UCLA). Timmons, J. carried out the majority of experiments, analysis, and writing as primary author. Falzone, G. contributed analysis and manuscript revisions. Balonis, M. contributed manuscript feedback and revisions. Bauchy, M. contributed to writing sections of the text and overall advising. Sant, G. was Principal Investigator.

ACKNOWLEDGEMENTS

Chapter 3 is a version of a manuscript in preparation for publication: Timmons, J., Mehdipour, I., Gao, S., Atahan, H., Neithalath, N., Bauchy, M., Garboczi, E., Srivastava, S., and Sant, G., 2019. Dispersing nanosized portlandite particulates via electrosteric exclusion at short screening lengths. The authors acknowledge financial support for this research from the National Science Foundation (DMREF: 1922167, CMMI: 1562066, CAREER: 1253269), Department of Energy: Office of Fossil Energy via the National Energy Technology Laboratory (NETL; DE-FE0029825 and DE-FE0031718), The Anthony and Jeanne Pritzker Family Foundation, and TRANSCEND: A joint UCLA-NIST Consortium that is funded by its industry and agency partners. Timmons, J. and Mehdipour, I. contributed equally to the manuscript, contributing the majority of experiments, analysis, and writing. Gao, S. conducted some experiments and provided analysis and writing concerning their results. Atahan, H. conducted many preliminary experiments which culminated in this study. Neithalath, N., Bauchy, M., and Garboczi, E. contributed advising and manuscript feedback. Srivastava, S. contributed to writing sections of the text and overall advising. Sant, G. was Principal Investigator.

CHAPTER 1

Introduction

Rheology is the study of flow and deformation of materials and is complementary to solid mechanics when describing the response of materials to applied forces. The most commonly discussed rheological properties include viscosity and yield stress. Suspension rheology specifically refers to solid particles, generally on the micrometer-scale or smaller, within a suspending (fluid) medium. Interparticle interactions, which account for the mutual attraction/repulsion between pairs of particles across the suspending medium, control the rheological properties of suspensions. Many properties of the particles will affect rheology, such as shape, size, and surface charge; these factors will determine if particles are dispersed and stable in suspensions or unstable and aggregate. Aggregates form when particles have insufficient repulsive interactions, resulting in increased viscosity, yield stress, and settling of particles. Control over these properties is important in the application of concentrated suspensions.

Studying model suspensions is often necessary to isolate how certain material properties affect rheology. Analysis of particle aggregates is simplest when the particles are spheres, removing any effects of ordered or preferential aggregation. The selection of suspending fluid is important, as it will control both electrostatic and van der Waals interactions between particles. Many parameters which affect aggregation and rheology are very difficult to quantify experimentally, and there are a variety of rheometric techniques to indirectly probe things like aggregate structure and interparticle interactions.

The rheology of generic mineral suspensions is important in a huge number of industries. For example, the mining industry produces a huge amount of mineral waste. These waste streams, known as tailings, are stored in tailings dams, which

take up huge tracts of land and are prone to catastrophic failure. Over the past century, thousands of people have been killed, millions of cubic meters of waste have been released into the environment, and billions of dollars in damages have been caused by tailings dam failures. A simple way to reduce the risk of failure is to simply reduce the volume of waste produced by lowering the water demand to produce a suspension which can be pumped to the waste site. But simply increasing the concentration of solids in the waste stream presents a host of new problems, stemming from increased yield stress, viscosity, and non-Newtonian behavior. Using polymeric additives which allow for flow of suspensions at higher solid particle loadings can combat these issues. Further examples of the importance of suspension rheology are discussed within the following chapters.

In Chapter 2, a model suspension of glass spheres in nonconductive polymer fluid is investigated. The fractal structure of the aggregates is shown to control the temperature dependence of the suspension viscosity, resulting in a viscous activation energy which deviates from predictions. In Chapter 3, a real suspension of portlandite (calcium hydroxide; $Ca(OH)_2$) in aqueous suspensions is shown to aggregate despite commonly-held guidelines which predict the stability of suspensions. This resulted in a very high yield stress at relatively low particle concentrations, undesirable properties for a suspension to be used as a structural material. By addition of polymeric dispersants, these properties can be tuned by altering the interparticle interactions due to surface modification by adsorbed polymers. These two investigations discuss the importance of understanding the aggregation of particles, as it is often the aggregate structure which connects particle properties to the rheology of the suspension.

CHAPTER 2

Anomalous variations in the viscous activation energy of suspensions induced by fractal structuring

Anomalous variations in the viscous activation energy of suspensions induced by fractal structuring

Jason Timmons ([1],[2]), Gabriel Falzone ([*],[†]), Magdalena Balonis ([†]), Mathieu Bauchy ([3]), and Gaurav Sant ([*],[†],[4])

Abstract

Hypothesis

In suspensions, the activation energy of viscous flow is an important property that controls the temperature dependence of the viscosity. However, the differentiated roles of the properties of the liquid phase and the structure of the solid particles in controlling the activation energy remain unclear. We propose here that particle fractal structuring yields an anomalous behavior in the activation energy of viscous flow.

Experiments

The rheology of two series of suspensions consisting of glass beads suspended in poly(1-decene) was investigated over a wide range of solid volume fractions ($0.00 \leq \varphi \leq 0.55$). These suspensions were characterized by their viscosity (η, Pa·s) via shear rate sweeps and by their yield stress (Pa) via oscillatory amplitude sweeps.

Findings

Interestingly, for suspensions consisting of nominally smaller particles ($d_{50} \approx 5$ μm), we observe an anomalous decrease in the activation energy (E_a, kJ/mol) of viscous flow with increasing solid fraction. Based on oscillatory rheology analyses, it is

[1] Laboratory for the Chemistry of Construction Materials (LC[2]), Department of Civil and Environmental Engineering, University of California, Los Angeles, CA, USA

[2] Department of Materials Science and Engineering, University of California, Los Angeles, CA, USA

[3] Laboratory for the Physics of Amorphous and Inorganic Solids (PARISlab), Department of Civil and Environmental Engineering, University of California, Los Angeles, CA, USA

[4] California Nanosystems Institute, University of California, Los Angeles, CA, USA

Corresponding authors: M. Bauchy (Email: bauchy@ucla.edu) and G. Sant (Email: gsant@ucla.edu)

suggested that such anomalous behavior arises due to entropic effects that result from the formation of fractally-architected cooperatively rearranging regions (i.e., agglomerates) in the suspension**.**

Keywords

Suspension rheology; fractal structuring; activation energy; configurational entropy

1. Introduction and background

When solid particles are added to a liquid, a suspension is formed. The continued addition of solid particles results in a drastic alteration of the rheological behavior of the suspension vis-à-vis the pure liquid [1]. Increasing the solid volume of the suspension monotonically increases its viscosity, regardless of the viscosity of the pure liquid [1,2]. The viscosity is influenced by numerous factors, including, but not limited to: temperature, pressure, particle volume fraction, particle size, and composition, shear rate, et cetera [1–8]. Substantial work has been carried out to describe the viscosity of simple suspensions of monodisperse hard spheres in the colloidal size regime [1–3,9–13]. However, the insights offered by experiments and simulations performed on such ideal systems may not be fully applicable to more complex suspensions of industrial relevance.

Like with pure liquids, the viscosity of a suspension decreases with increasing temperature [14]. In the ranges of temperatures that are distant from those that may cause a phase transition in the solid or liquid phases of the suspension, the influence of temperature on the suspension viscosity is broadly induced by changes

in the liquid phase viscosity [15]. But, for colloidal-sized particles, the thermal forces (k_BT) acting on the particles can prevent their settling [16]. In commonality with many other properties, the influence of temperature on the viscosity of a suspension can be described by an Arrhenius equation involving an activation energy of flow E_A (see Eq. 1) [17]. This activation energy has most often found to be independent of the solid volume fraction, which indicates that it is indeed the liquid phase that, to the first-order, controls the temperature-dependence of the suspension viscosity [13,18]. While other investigations have sought to relate the activation energy to particle volume, the mechanism(s) that may underpin such correlations remain unclear [19,20].

Besides the viscosity, the storage and loss moduli of a suspension, which capture the elastic and viscous character of the material, respectively, describe how the structure of a suspension breaks down and evolves with increasing shear strain [21]. At very low shear strain, the storage modulus of a structured, yielding suspension should plateau to a constant value, and this value is expected to scale with the solid volume fraction [21–23]. As more solid particles are added to the system, the system behaves more like an elastic solid, and up on its continued shearing, the storage modulus begins to decrease, which is known as yielding [21–23]. The strain and stress at which yielding occurs are defined as the critical yielding strain (γ_c) and yield stress (τ_c), respectively [22–24]. Beyond this point, the material undergoes viscous flow. Depending on the structuring of the particles in the suspension, the yield strain and yield stress scale differently with solid volume fraction [21,23,25,26].

Despite the tremendous importance of the rheology of suspensions (e.g., for the food, cosmetic, pharmaceutical, or oil industries)[27–31], the many variables that may affect rheological properties are difficult to reconcile with a description of the suspension structure [32]. For example, common models, such as those of Einstein, Batchelor, and Krieger and Dougherty, depend solely on the solid volume fraction of the suspension [9–11,33], and do not explicitly account for the role of suspension structure—a significant issue, especially for concentrated suspensions (often, $\varphi \geq 0.15 - 0.20$) [34]—and therefore fail to describe the rheology of many suspensions [9–11]. In particular, the average size of the suspended particles and the structuring of the particles in the suspension have a first-order effect on the structure and rheology of suspensions and, hence, should be explicitly accounted for in a unifying model of suspension rheology. Using simulations, suspensions comprising polydisperse particles have been shown to weakly differ in terms of fractal structuring [35,36]. However, beyond the two prevailing models of diffusion- and reaction-limited cluster aggregation, the effect of structuring on the rheological properties of suspensions remains difficult to predict [36,37].

Here, we investigate two sets of suspensions comprising two sizes of solid glass beads suspended in a poly(1-decene) solution over a range of temperatures and solid volume fractions. We observe an anomalous response in the temperature dependence of the viscosity for the suspension consisting of smaller beads, wherein the activation energy decreases with increasing solid volume fraction. Based on oscillatory rheology analyses, we find that this anomalous behavior originates from the fractal nature of the agglomerates (or cooperatively rearranging regions) that

form in the suspension. Using Adam-Gibbs theory [38], we show that the average size of the agglomerates affects the configurational entropy of the system, which, in turn, controls the activation energy of shear flow. This highlights the considerable role of entropic effects (i.e., besides enthalpic effects) in controlling and affecting the rheology of complex suspensions.

2. Materials and methods

2.1 Materials

Two sets of soda-lime silicate (SLS) glass beads (SiLibeads Type S 0-20 and 0-50, Sigmund-Lindner GmbH) of different sizes were used as model spherical particles. The oxide composition of both sets of the SLS glass beads as determined by SEM-EDS is 69.5 mol % SiO_2, 14.7 mol % Na_2O, 10.3 mol % CaO, 4.8 mol % MgO, 0.4 mol % Al_2O_3, and 0.3 mol % K_2O. Approximately 92.5% of particles are spherical, featuring an aspect ratio of: 1.00 ± 0.05, with the remaining 7.5% of particles having an irregular shape with aspect ratios ranging from 1.0-to-5.0, based on analysis of 120 particles from SEM images, thereby fulfilling the condition of a spherical geometry (see Supplementary Information, SI)[2,3,11]. The median diameter (d_{50}) of the smaller glass beads and the larger glass beads are 5.0 ± 0.3 μm and 28 ± 0.3 μm, respectively, wherein the error represents one standard deviation based up on 6 replicate measurements. These particle sizes were chosen to approach the particle size at which thermal forces become dominant in controlling particle motion. The particle size distributions (PSDs) of the glass beads were determined by static light scattering (SLS, LS13-320, Beckman Coulter). For the PSD measurements, Isopropyl alcohol (IPA) was used as the carrier fluid and the mixture of IPA and the SLS beads

was extensively ultrasonicated prior to the measurements to ensure dispersion to primary particles [39]. The density of the glass beads was measured by He-pycnometry (AccuPyc II TEC, Micromeritics) to be 2450 kg/m^3. To confirm that both sets of glass beads had similar surface properties, the zeta potential of each in deionized water was measured by electrophoretic mobility (ZetaPALS, Brookhaven Instruments Corporation) and both were found to be -43 ± 3 mV.

A set of polyethylene beads (WPMS-1.25 10-45 μm, Cospheric LLC) were also used, to compare the results of similarly-sized and similarly-shaped particles with different material properties. The d_{50} of these particles are 30 ± 0.3 μm, closely matching that of the 28 μm glass beads. The density, as reported by the manufacturer, is 1239 kg/m^3, resulting in a much smaller density mismatch between the particles and the suspending fluid, described below.

A NIST-certified viscosity standard (S600, Cannon Instruments) was used as the continuous phase of the suspension (i.e., suspending liquid which is poly(1-decene) with a unique molecular weight distribution). S600 was selected for its high viscosity (1.02 Pa·s at 25 °C), which was necessary to prevent particle settling and sedimentation over the timescale of the experiments. This selection ensured very good repeatability of the rheological measurements (i.e., we observed a maximum 2% deviation in viscosity between three repetitions on the pure fluid) and a suspending medium which would not react with or cause dissolution of the suspended solids.

Three sets of suspensions of the 5.0 μm and 28 μm glass beads and 30 μm polyethylene beads (discrete phase) and S600 liquid (continuous phase) were prepared over a range of solid volume fractions ($0.00 \leq \varphi \leq 0.55$) and studied over a range of temperatures (from T = 25-to-80 °C). Since the density of the fluid changes with temperature, these volume fractions slightly change ($\Delta\varphi \leq 0.01$) for experiments conducted at the highest temperature considered herein (80 °C). In the following, this difference is assumed to be insignificant and, is hence neglected. Suitable quantities of solid and S600 liquid were measured using an analytical balance (0.1 mg precision) assuming nominal densities of 2450 kg/m^3, 1239 kg/m^3, and 843.8 kg/m^3 for the glass beads, polyethylene beads, and liquid, respectively. The suspensions were homogenized using a four-blade impeller type standing mixer (RW 20 Digital, IKA) at 300 rpm for five minutes prior to further analyses.

2.2 Experimental methods

The rheology of the suspensions was characterized using a combined motor and transducer (CMT) rheometer (Discovery Hybrid Rheometer, DHR-2, TA Instruments). A Couette-type rotor with a convex conical end was used as the upper geometry in a concentric-cylinder setup. The shear viscosity was examined at three temperatures (T = 25 ± 0.1, 40 ± 0.1, and 80 ± 0.1 °C). The temperature was controlled via a Peltier concentric cylinder jacket that surrounds the geometry. This temperature range was selected to: (i) provide verification of the viscosity measured in the pressure cell with respect to the NIST reference values, (ii) remain below the flashpoint of the S600 liquid (i.e., < 224 °C), and (iii) prevent condensation that may

occur at sub-ambient temperatures, and which may introduce water in to the suspension.

For each experiment, the sample geometry was first loaded with 22 ± 1.0 mL of the suspension. The sample was brought to 25 ± 0.1 °C and held for ten minutes prior to initiation of shearing—to minimize temperature gradients. Following sample loading and temperature equilibration, a shear strain rate ($\dot{\gamma}$) sweep was conducted from $\dot{\gamma}$ = 0.1 to 500 s^{-1} for five points per decade, without any pre-shear. At each of these five unique logarithmically-stepped shear strain rates within each decade, the shear strain rate was maintained for a period of 60 s, during which the torque was recorded every 10 s. Steady-state sensing was used so that an "equilibrated" reading was considered to have been obtained only if the torque varied by less than 5% over three consecutive measurements. If this criterion was not fulfilled, the data reported was derived from the average torque measured over the experimental duration. A single measurement could take a minimum of 30 s and a maximum of 60 s. This nature of rheological characterization was carried out at each different isothermal temperature of interest. Following the characterizations at each temperature, an additional test at 25 ± 0.1 °C was performed after 15 minutes (that is, the time needed to lower the temperature from 80 to 25 °C) to verify that neither the temperature variations nor the shear history imposed on the suspension did not result in irreversible modifications of its rheological response. The flow curves obtained from these measurements are reported in the SI.

A rheological method was used to determine the fractal dimension of the aggregates in suspension [21,23]. This method was chosen on account of its simplicity and to show that suspensions can be characterized very well through solely rheological methods. Additionally, this method presents some advantages over alternative methods, e.g., image analysis (which can only quantify fractal dimension of ≤ 2) or light scattering (which relies on a complex analysis of the results and is best applied to micron-size particles only) [36].

Oscillatory rheological measurements were conducted using the concentric cylinder setup to measure storage and loss moduli, yield strain (see SI), and yield stress of the suspensions. The suspension as loaded into the cell and the temperature equilibrated to 25 ± 0.1 °C. A preshearing step was carried out at a strain rate of 100 s^{-1} for five minutes to simulate a shear history imparted by the lengthier shear sweep experiments described above, after which the sample was allowed to rest for 60 seconds before the start of the oscillatory measurements. Oscillation amplitude sweeps were conducted such that the rheometer head oscillated at a frequency of 10 rad/s to impose a given strain on the sample—the strain being logarithmically-spaced from 0.001% to 20%. Each strain step was measured in intervals of 6.5 ± 0.1 s. The storage modulus and loss modulus were then calculated from the measured phase angles. Such oscillatory characterization were also carried out at an isothermal temperature of 80 ± 0.1 °C.

3. Results

The relative viscosity $\eta_r = \eta/\eta_f$ (i.e., normalized by the viscosity of the fluid η_f) of each of the two series of suspensions (i.e., of 5 μm and 28 μm glass beads) is shown in **Fig. 1**. Expectedly, we observe that the relative viscosity increases with solid volume fraction. In addition, we note that temperature has a significantly different effect on the two series of suspensions. For example, while the relative viscosity of the 28 μm particle series is only slightly affected by temperature at a given solid volume fraction (**Fig. 1b**), temperature strongly alters the relative viscosity of the 5 μm glass bead series (**Fig. 1a**) at a given solid content [12]. This suggests that, in the latter case, the temperature dependence of the viscosity of the suspension is not only a function of the temperature-dependence of the viscosity of the liquid phase [15]. As shown in **Fig. 2(a-b)**, we observe that, in general, the suspension viscosity decreases with increasing temperature, and the suspension viscosity, η demonstrates Arrhenius-like behavior [17]:

$$\eta = \eta_0 \exp\left(\frac{E_a}{RT}\right) \qquad \textbf{Equation (1)}$$

where, η_0 is a prefactor (i.e., the viscosity at "infinite temperature"), E_a *is* the activation energy of viscous flow, and *R* is the universal gas constant. Across both series of suspensions, we observe that the prefactor η_0 increases with increasing solid volume fraction. This observation contrasts with most conventional liquids, for which the "infinite temperature" viscosity η_0 is often found to be a constant [40]. Interestingly, we note that, although the slope of the Arrhenius plots of the viscosity of the 28 μm particle system remains largely unaffected by the solid volume fraction (see **Fig. 2b**), the slope of the Arrhenius plots for the 5 μm particle system (**Fig. 2a**)

diminishes with increasing solid content. This suggests that, unexpectedly, and anomalously, the addition of 5 μm particles reduces the temperature dependence of viscous flow, and hence the activation energy E_a of these suspensions. The contact angle of the liquid phase on a soda-lime glass slide, i.e., similar to the glass beads used herein, was measured to be 32°, ruling out the existence of a strongly unfavorable interface between the two phases. The contact angle on a polyethylene surface was found to be ~10°, indicating that the interface is even more energetically favorable.

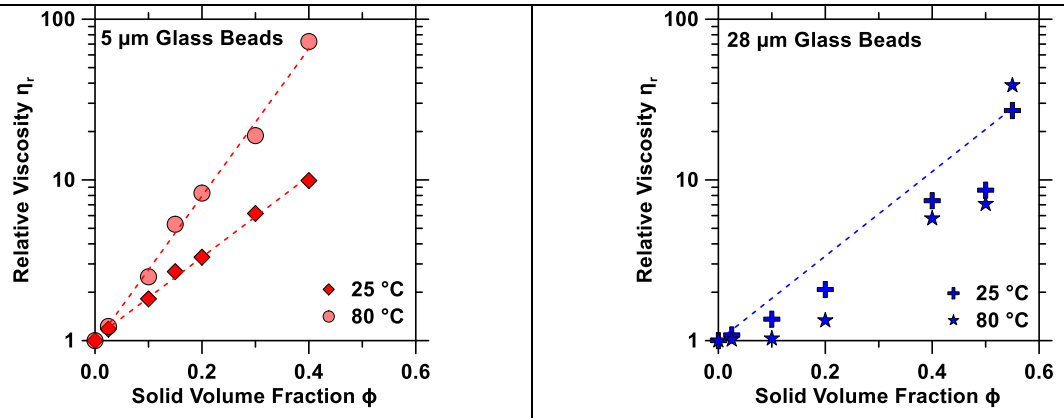

(a) **(b)**

Figure 1: The relative viscosity (i.e., normalized by the viscosity of the liquid phase) of the two series of suspensions as a function of the solid volume fraction at 25 ± 0.1 °C and 80 ± 0.1 °C. The dashed lines are shown to guide the eye.

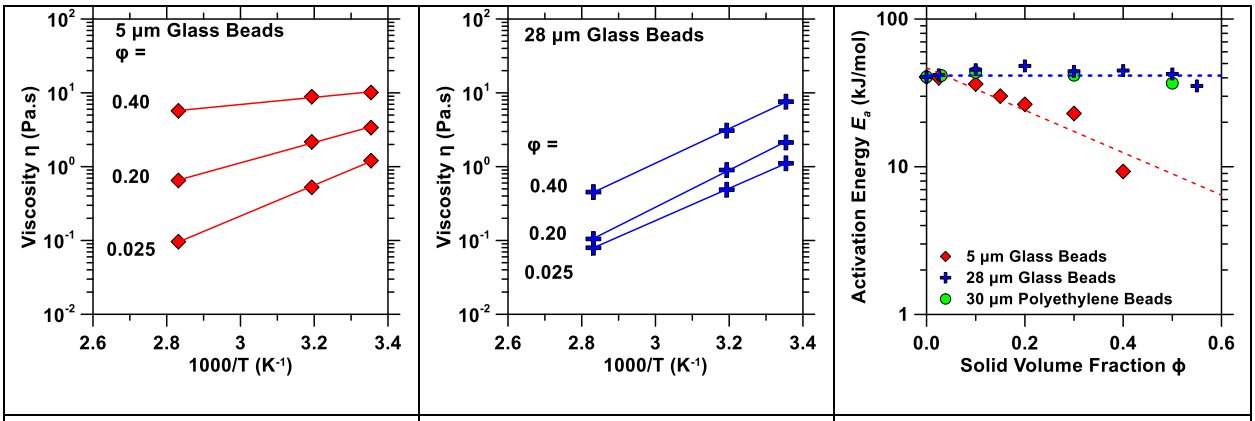

Figure 2: (a-b) Arrhenius plots of the suspension viscosity for suspensions constituted using: **(a)** 5 μm, and, **(b)** 28 μm glass beads for selected solid volume fractions. The data are fitted by an Arrhenius expression (see **Eq. 1**). **(c)** The activation energy of viscous flow of the suspensions as a function of the solid volume fraction. The dashed lines show the general trend of the dataset.

The evolution of the activation energy of viscous flow (E_a, i.e., as obtained by fitting the curves presented in **Fig. 2(a-b)** with **Eq. 1**) is shown in **Fig. 2(c)**. First, we observe that the activation energy remains largely unaffected by solid volume fraction for the 28 μm particle suspensions—i.e., expected behavior when the viscosity of the suspension (and its temperature dependence) is controlled by the temperature-dependence of the viscosity of the liquid phase [15]. In contrast, the 5 μm glass bead suspensions exhibit an anomalous response, namely, the activation energy of viscous flow decreases in a near-linearly with increasing solid content. The behavior of the 28 μm glass beads is closely matched by that of the 30 μm polyethylene beads, suggesting that the alternative behavior exhibited by the 5 μm glass beads is a result of the particle size, and not of the material itself. This is

highlighted to be on account of the suspension structure as noted in the text that follows.

4. Discussion

To explain the anomalous trends in the activation energy of viscous flow, we rely on the power-law scaling theory of Shih *et al.* [21]—following the procedure recently outlined by Liberto *et al.* [23]—to evaluate the structure of the suspension. This framework relies on a fractal description of the suspension and describes the relationship between its structure and yielding behavior. As such, within this framework, the suspension's yield stress τ_c is assumed to scale with the solid volume fraction φ with a power law exponent *C*:

$$\tau_c \propto \phi^C \qquad \textbf{Equation (2)}$$

where, the scaling exponent *C* is a function of the fractal dimension d_f of the solid structure in the suspension:

$$C = \frac{2}{3 - d_f} \qquad \textbf{Equation (3)}$$

Fig. 3(a) shows the yield stress τ_c of both suspension series as a function of the solid volume fraction. As expected, we observe that, in both cases, τ_c increases with increasing solid content. However, we note that, at low solid volume fractions, the yield stress of the 28 μm glass bead system is essentially equal to that of the pure liquid. This suggests that this regime (i.e., at low values of yield stress) cannot be

described by the power-law scaling theory of Shih *et al.* [21] Beyond this regime however, as the yield stress sharply increases, the yield stress values were fitted using **Eq. 2** to determine the scaling coefficient (C), which, in turn, reveals the fractal dimension of the suspension (see **Eq. 3**). Following this approach, the fractal dimensions of each of the suspension series was found to be $d_{f,\ 5\ \mu m} = 2.54$ and $d_{f,\ 28\ \mu m} = 2.81$, respectively.

The fractal dimension is related to the packing efficiency of the particles within the agglomerates. Therefore, a value of $d_f = 3$ (i.e., the Euclidian dimension) indicates no fractal behavior wherein the particles either do not agglomerate (see **Fig. 3b**) or agglomerate into entirely close-packed assemblages—which would be here unlikely considering the size of the particles [25,26]. In contrast, values of $d_f \leq 3$ denote that the fractal character of the agglomerates increases (see **Fig. 3c**). As such, our results indicate that the 5 μm exhibits a substantial fractal behavior (i.e., $d_f \approx 2.5$), whereas the 28 μm glass bead system shows a relatively modest fractal behavior ($d_f = 2.81$), that is, much closer to the maximum value of $d_f = 3$. It should be noted that $d_f \approx 3$ indicates a ballistic regime, wherein the particles move in straight-line paths before colliding due their high inertia [41]. On the other hand, $d_f \approx 2.5$ suggests compliance with a thermal regime, wherein the particles exhibit a random-walk motion before forming agglomerations following their collision (i.e., diffusion-limited agglomeration) [42]. Overall, this suggests that the anomalous behavior of the 5 μm glass bead suspensions (i.e., of a reducing temperature dependence of viscous flow with increasing solid volume fraction) arises from the tendency of its particles to agglomerate in a fractal fashion.

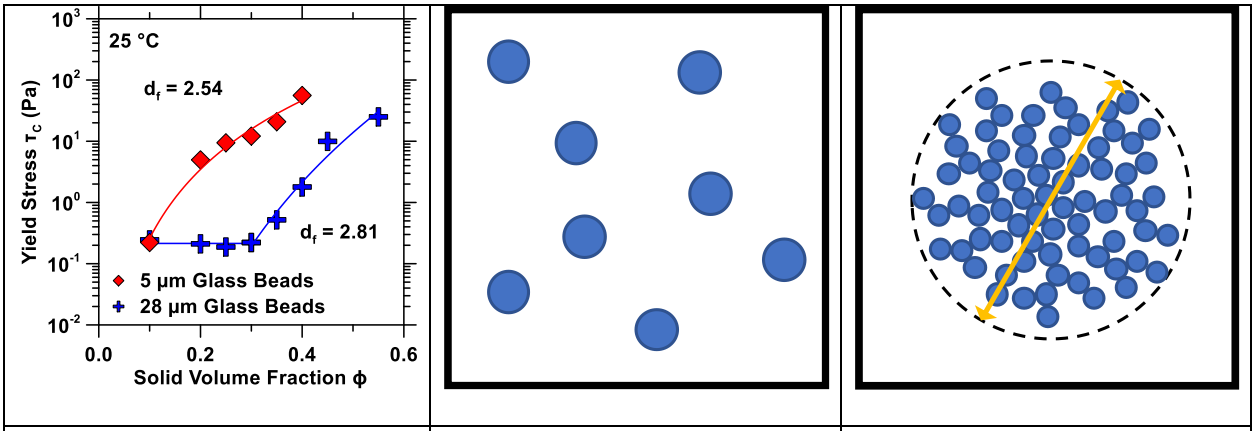

(a) **(b)** **(c)**

Figure 3: (a) The yield stress and the corresponding fractal dimension for the two different series of glass bead suspensions. For the 28 μm glass bead suspensions, power-law fits were only considered for $\varphi \geq 0.30$, where the system is concentrated enough that the scaling theory applies and a yield stress superior to the liquid's yield stress was measured. Representative schematics that illustrate the structure of a suspension exhibiting: **(b)** no agglomeration, and, **(c)** fractal agglomeration. The circle shows the characteristic length-scale of the fractal agglomerates.

We propose that the anomalous activation energy behavior reported herein can be explained in terms of an entropic effect that results from the formation of "cooperatively rearranging regions" (CRRs). As illustrated in **Fig. 3(c)**, agglomeration results in the formation of clusters of particles (i.e., agglomerates or flocs), which tend to move collectively rather than individually (i.e., they behave as CRRs). The impact of the formation of CRRs on the activation energy of shear flow

can then be understood within the framework of Adam–Gibbs theory [38], which is commonly used to describe the viscosity of glass-forming supercooled liquids as:

$$\eta = \eta_0 \exp\left(\frac{A}{TS_c}\right) \qquad \textbf{Equation (4)}$$

where, A is proportional to the activation energy of shear flow E_a in the absence of any CCRs and S_c is the configurational entropy. Within this framework, CRRs are defined as the smallest volume elements that can collectively relax in their environment. This suggests that the formation of a large number of CRRs would result in a decrease in the entropy S_c since the number of accessible configurations decreases. In turn, at a fixed temperature, a lower configurational entropy would result in an increase in the effective activation energy of the system. In the context of glass-forming supercooled liquids, an increase in the size of CRRs as temperature decreases explains the non-Arrhenius nature of their viscosity, i.e., since the effective activation energy is inversely proportional to S_c [38].

Contrastingly, in dispersed (i.e., non-agglomerated) suspensions, the size of the CRRs is constant and equivalent to the size of a single particle. Therefore, in such regimes, the activation energy of viscous flow is independent of the solid volume fraction. This is in line with the behavior of the 28 μm particle suspensions (see **Fig. 2c**), which experience relatively limited agglomeration. However, in agglomerated suspensions, the average size of the CRRs depends on the solid volume fraction. In fractal agglomerated gels, the average size L of the colloidal agglomerates (i.e., the CRRs) was found to scale with the solid volume fraction as [43]:

$$L \propto \phi^{-1/(3-d_f)}$$ **Equation (5)**

As such, for $d_f \approx 2.5$ (i.e., for the 5 μm particle suspensions), the average size of the CRRs given by L is expected to scale as ϕ^{-2}. Following Adam-Gibbs theory, this scaling implies that that an increase in the solid volume fraction ϕ results in an increase in the entropy S_c (i.e., and a reduced number of accessible fractal configurations for the individual agglomerates, or CRRs, likely due to volumetric crowding) which results in a decrease in the effective activation energy of the system. This is in line with the observed behavior of the 5 μm particle suspensions, which exhibit a decrease in the activation energy with increasing ϕ (see **Fig. 2c**). Taken together, these results support the idea that the anomalous behavior in the activation energy of viscous flow observed herein results from an entropic effect due to the formation of CRRs following flocculation.

5. Summary and conclusions

By combining previously reported analysis methods to critically examine the rheology of two series of suspensions constituted of particles that feature different median particle sizes [17,21,23], we report that smaller particles (5 μm glass beads) trigger an anomalous response in the activation energy of viscous flow, which is found to decrease with increasing solid fraction. We show that this anomalous behavior is associated with the formation of fractal agglomerates in the suspension and suggest that that this behavior arises from the fact that the agglomerates act as cooperatively rearranging regions (CRRs), whose size depends on the solid volume fraction. The

formation of such CRRs affects the configurational entropy of the system, which, in turn, controls the activation energy of shear flow, i.e., following the Adam–Gibbs equation [38].

Overall, these results highlight the benefits of relying on thermodynamic analyses to describe the crucial role of entropic effects in controlling the rheological properties of suspensions, and the critical role of particle size therein. This approach allows us to uncover some new understanding regarding how particle size and suspension fractal structure can alter the viscous activation energy of suspensions. This type of knowledge can, in turn, pave the way toward the design of novel suspensions that exhibit tailored viscous activation energy—e.g., a lower temperature-dependence of their rheology. The generality of the present findings should now be further established by investigating a wider range of systems, i.e., including various combinations of fluids and particles types. Indeed, the viscous activation energy of various systems has been reported to change with the particle size [44–47]. A thermodynamic analysis, as presented herein, could be conducted to revisit these systems and elucidate the structural and thermodynamical origin of the trends observed in previous studies. Additional investigations focusing on a wider range of particle sizes should be conducted to confirm that the anomalous behavior reported herein expands beyond the conditions explored in the present investigation. Applying the analytic framework developed herein to a more diverse set of systems will help to elucidate how the constituent material properties impact the rheological properties of suspensions and further demonstrate the importance of considering entropic effects within particle interactions.

Conflicts of Interest

There are no conflicts of interest to declare.

Acknowledgements

The authors acknowledge financial support for this research provisioned by the National Science Foundation (CMMI: 1401533, 1562066, CAREER Award: 1253269), and University of California, Los Angeles (UCLA). The contents of this paper reflect the views and opinions of the authors who are responsible for the accuracy of datasets presented herein. This research was carried out in the Laboratory for the Chemistry of Construction Materials (LC^2) and Molecular Instrumentation Center at UCLA. As such, the authors gratefully acknowledge the financial support that has made these laboratories and their operations possible. The authors acknowledge insightful discussions with Dr. Iman Mehdipour and Dr. Monday U. Okoronkwo who are gratefully acknowledged.

References

[1] S. Mueller, E.W. Llewellin, H.M. Mader, The rheology of suspensions of solid particles, Proc. R. Soc. Lond. Math. Phys. Eng. Sci. (2009) rspa20090445. doi:10.1098/rspa.2009.0445.

[2] M. Mooney, The viscosity of a concentrated suspension of spherical particles, J. Colloid Sci. 6 (1951) 162–170. doi:10.1016/0095-8522(51)90036-0.

[3] C.G. de Kruif, E.M.F. van Iersel, A. Vrij, W.B. Russel, Hard sphere colloidal dispersions: Viscosity as a function of shear rate and volume fraction, J. Chem. Phys. 83 (1985) 4717–4725. doi:10.1063/1.448997.

[4] F. Yziquel, P.J. Carreau, M. Moan, P.A. Tanguy, Rheological modeling of concentrated colloidal suspensions, J. Non-Newton. Fluid Mech. 86 (1999) 133–155. doi:10.1016/S0377-0257(98)00206-7.

[5] R.C. Navarrete, L.E. Scriven, C.W. Macosko, Rheology and Structure of Flocculated Iron Oxide Suspensions, J. Colloid Interface Sci. 180 (1996) 200–211. doi:10.1006/jcis.1996.0290.

[6] P. Coussot, C. Ancey, Rheophysical classification of concentrated suspensions and granular pastes, Phys. Rev. E. 59 (1999) 4445–4457. doi:10.1103/PhysRevE.59.4445.

[7] J. Bergenholtz, Theory of rheology of colloidal dispersions, Curr. Opin. Colloid Interface Sci. 6 (2001) 484–488. doi:10.1016/S1359-0294(01)00112-1.

[8] W.C.K. Poon, The physics of a model colloid–polymer mixture, J. Phys. Condens. Matter. 14 (2002) R859. doi:10.1088/0953-8984/14/33/201.

[9] A. Einstein, Eine neue Bestimmung der Moleküldimensionen, Ann. Phys. 324 (1906) 289–306. doi:10.1002/andp.19063240204.

[10] G.K. Batchelor, The effect of Brownian motion on the bulk stress in a suspension of spherical particles, J. Fluid Mech. 83 (1977) 97–117. doi:10.1017/S0022112077001062.

[11] I.M. Krieger, T.J. Dougherty, A Mechanism for Non-Newtonian Flow in Suspensions of Rigid Spheres, Trans. Soc. Rheol. 3 (1959) 137–152. doi:10.1122/1.548848.

[12] D.B. Genovese, Shear rheology of hard-sphere, dispersed, and aggregated suspensions, and filler-matrix composites, Adv. Colloid Interface Sci. 171–172 (2012) 1–16. doi:10.1016/j.cis.2011.12.005.

[13] S.H. Maron, P.E. Pierce, Application of ree-eyring generalized flow theory to suspensions of spherical particles, J. Colloid Sci. 11 (1956) 80–95. doi:10.1016/0095-8522(56)90023-X.

[14] O. Reynolds, IV. On the theory of lubrication and its application to Mr. Beauchamp tower's experiments, including an experimental determination of the viscosity of olive oil, Philos. Trans. R. Soc. Lond. 177 (1886) 157–234. doi:10.1098/rstl.1886.0005.

[15] J.S. Chong, E.B. Christiansen, A.D. Baer, Rheology of concentrated suspensions, J. Appl. Polym. Sci. 15 (1971) 2007–2021. doi:10.1002/app.1971.070150818.

[16] J.F. Richardson, W.N. Zaki, The sedimentation of a suspension of uniform spheres under conditions of viscous flow, Chem. Eng. Sci. 3 (1954) 65–73. doi:10.1016/0009-2509(54)85015-9.

[17] H.D. Chandler, Activation entropy and anomalous temperature dependence of viscosity in aqueous suspensions of Fe2O3, Powder Technol. 305 (2017) 572–577. doi:10.1016/j.powtec.2016.10.036.

[18] S.K. Mishra, P.K. Senapati, D. Panda, Rheological Behavior of Coal-Water Slurry, Energy Sources. 24 (2002) 159–167. doi:10.1080/00908310252774471.

[19] N. Grigelmo-Miguel, A. Ibarz-Ribas, O. Martín-Belloso, Rheology of peach dietary fibre suspensions, J. Food Eng. 39 (1999) 91–99. doi:10.1016/S0260-8774(98)00151-4.

[20] G.D. Saravacos, Effect of Temperature on Viscosity of Fruit Juices and Purees, J. Food Sci. 35 (1970) 122–125. doi:10.1111/j.1365-2621.1970.tb12119.x.

[21] W.-H. Shih, W.Y. Shih, S.-I. Kim, J. Liu, I.A. Aksay, Scaling behavior of the elastic properties of colloidal gels, Phys. Rev. A. 42 (1990) 4772–4779. doi:10.1103/PhysRevA.42.4772.

[22] N. Koumakis, G. Petekidis, Two step yielding in attractive colloids: transition from gels to attractive glasses, Soft Matter. 7 (2011) 2456–2470. doi:10.1039/C0SM00957A.

[23] T. Liberto, M.L. Merrer, C. Barentin, M. Bellotto, J. Colombani, Elasticity and yielding of a calcite paste: scaling laws in a dense colloidal suspension, Soft Matter. 13 (2017) 2014–2023. doi:10.1039/C6SM02607A.

[24] Yielding of colloidal glasses, EPL Europhys. Lett. 75 (2006) 624. doi:10.1209/epl/i2006-10156-y.

[25] D.W. Schaefer, J.E. Martin, P. Wiltzius, D.S. Cannell, Fractal Geometry of Colloidal Aggregates, Phys. Rev. Lett. 52 (1984) 2371–2374. doi:10.1103/PhysRevLett.52.2371.

[26] R.K. Chakraborti, K.H. Gardner, J.F. Atkinson, J.E. Van Benschoten, Changes in fractal dimension during aggregation, Water Res. 37 (2003) 873–883. doi:10.1016/S0043-1354(02)00379-2.

[27] M.A. Rao, Rheology of Liquid Foods - a Review, J. Texture Stud. 8 (1977) 135–168. doi:10.1111/j.1745-4603.1977.tb01173.x.

[28] H.-J. Buschmann, E. Schollmeyer, Applications of cyclodextrins in cosmetic products: A review, J. Cosmet. Sci. 53 (2002) 185–191.

[29] B.E. Rabinow, Nanosuspensions in drug delivery, Nat. Rev. Drug Discov. 3 (2004) 785. doi:10.1038/nrd1494.

[30] R. Martínez-Palou, M. de L. Mosqueira, B. Zapata-Rendón, E. Mar-Juárez, C. Bernal-Huicochea, J. de la Cruz Clavel-López, J. Aburto, Transportation of heavy and extra-heavy crude oil by pipeline: A review, J. Pet. Sci. Eng. 75 (2011) 274–282. doi:10.1016/j.petrol.2010.11.020.

[31] M. He, Y. Wang, E. Forssberg, Slurry rheology in wet ultrafine grinding of industrial minerals: a review, Powder Technol. 147 (2004) 94–112. doi:10.1016/j.powtec.2004.09.032.

[32] J. Mewis, N.J. Wagner, Current trends in suspension rheology, J. Non-Newton. Fluid Mech. 157 (2009) 147–150. doi:10.1016/j.jnnfm.2008.11.004.

[33] I.M. Krieger, Rheology of monodisperse latices, Adv. Colloid Interface Sci. 3 (1972) 111–136. doi:10.1016/0001-8686(72)80001-0.

[34] J.F. Brady, G. Bossis, The rheology of concentrated suspensions of spheres in simple shear flow by numerical simulation, J. Fluid Mech. 155 (1985) 105–129. doi:10.1017/S0022112085001732.

[35] M. Tence, J.P. Chevalier, R. Jullien, On the measurement of the fractal dimension of aggregated particles by electron microscopy : experimental method, corrections and comparison with numerical models, J. Phys. 47 (1986) 1989–1998. doi:10.1051/jphys:0198600470110198900.

[36] G.C. Bushell, Y.D. Yan, D. Woodfield, J. Raper, R. Amal, On techniques for the measurement of the mass fractal dimension of aggregates, Adv. Colloid Interface Sci. 95 (2002) 1–50. doi:10.1016/S0001-8686(00)00078-6.

[37] G. Bushell, R. Amal, Fractal Aggregates of Polydisperse Particles, J. Colloid Interface Sci. 205 (1998) 459–469. doi:10.1006/jcis.1998.5667.

[38] G. Adam, J.H. Gibbs, On the Temperature Dependence of Cooperative Relaxation Properties in Glass-Forming Liquids, J. Chem. Phys. 43 (1965) 139–146. doi:10.1063/1.1696442.

[39] K.-Y. Chu, A.R. Thompson, Densities and Refractive Indices of Alcohol-Water Solutions of n-Propyl, Isopropyl, and Methyl Alcohols., J. Chem. Eng. Data. 7 (1962) 358–360. doi:10.1021/je60014a011.

[40] J.C. Mauro, Y. Yue, A.J. Ellison, P.K. Gupta, D.C. Allan, Viscosity of glass-forming liquids, Proc. Natl. Acad. Sci. 106 (2009) 19780–19784. doi:10.1073/pnas.0911705106.

[41] R.C. Ball, T.A. Witten, Particle aggregation versus cluster aggregation in high dimensions, J. Stat. Phys. 36 (1984) 873–879. doi:10.1007/BF01012946.

[42] P. Meakin, S. Tolman, Fractals in the natural sciences - Diffusion-limited aggregation, Proc R Soc Lond A. 423 (1989) 133–148. doi:10.1098/rspa.1989.0046.

[43] P.-G. de Gennes, Scaling Concepts in Polymer Physics, Cornell University Press, 1979.

[44] F. Abbès, M. Masmoudi, W. Kchaou, S. Danthine, C. Blecker, H. Attia, S. Besbes, Effect of enzymatic treatment on rheological properties, glass temperature transition and microstructure of date syrup, LWT - Food Sci. Technol. 60 (2015) 339–345. doi:10.1016/j.lwt.2014.08.027.

[45] S.P. Yadav, R. Manohar, S. Singh, Effect of TiO2 nanoparticles dispersion on ionic behaviour in nematic liquid crystal, Liq. Cryst. 42 (2015) 1095–1101. doi:10.1080/02678292.2015.1025872.

[46] Maggi Filippo, Curing Viscosity of HTPB-Based Binder Embedding Micro- and Nano-Aluminum Particles, Propellants Explos. Pyrotech. 39 (2014) 755–760. doi:10.1002/prep.201400010.

[47] S.B. Rekik, S. Gassara, J. Bouaziz, A. Deratani, S. Baklouti, Development and characterization of porous membranes based on kaolin/chitosan composite, Appl. Clay Sci. 143 (2017) 1–9. doi:10.1016/j.clay.2017.03.008.

CHAPTER 3

Dispersing nanosized portlandite particulates via electrosteric exclusion at short screening lengths

Dispersing nanosized portlandite particulates via electrosteric exclusion at short screening lengths

Jason Timmons ([5],[6],[+]), Iman Mehdipour ([2],[+]), Shang Gao ([7]), Hakan Atahan ([6],[8]), Narayanan Neithalath ([9]), Mathieu Bauchy ([10],[13]), Edward Garboczi ([11]), Samanvaya Srivastava ([3],[13],[**]), Gaurav Sant ([5],[6],[12],[13],[**])

Abstract

In spite of their high surface charge (ζ = +34 mV), aqueous suspensions of portlandite (calcium hydroxide: $Ca(OH)_2$) exhibit a strong tendency to aggregate, and thereby present unstable suspensions. While a variety of commercial dispersants seek to affect suspension stability, and rheology (e.g., yield stress, viscosity) it remains unclear whether electrostatically, and/or electrosterically based additives may be most effective additives. We show that the high native ionic strength (and pH ≈ 12.6, IEP: pH ≈ 13) of portlandite suspensions strongly screens electrostatic forces (Debye length: κ^{-1} = 1.2 nm); as a result of which simple Coulombic repulsion alone is insufficient to affect rheology. On the other hand, the longer-range geometrical particle-particle exclusion that arises from electrosteric

[5] Department of Materials Science and Engineering, University of California, Los Angeles, CA 90095, USA
[6] Laboratory for the Chemistry of Construction Materials (LC^2), Department of Civil and Environmental Engineering, University of California, Los Angeles, CA 90095, USA
[7] Department of Chemical and Biomolecular Engineering, University of California, Los Angeles, CA 90095, USA
[8] Department of Civil Engineering, Istanbul Technical University, Istanbul, Turkey
[9] School of Sustainable Engineering and the Built Environment, Arizona State University, Tempe, AZ 86587, USA
[10] Laboratory for the Physics of Amorphous and Inorganic Solids (PARISlab), Department of Civil and Environmental Engineering, University of California, Los Angeles, CA 90095, USA
[11] Applied Chemicals and Materials Division, Material Measurement Laboratory, National Institute of Standards and Technology, Boulder, CO 80305, USA
[12] California Nanosystems Institute (CNSI), University of California, Los Angeles, CA 90095, USA
[13] Institute for Carbon Management, University of California, Los Angeles, CA 90095, USA

[+] Both authors contributed equally to this work.

[**]Corresponding authors: S. Srivastava, Email: samsri@ucla.edu and G. Sant, Email: gsant@ucla.edu

hindrance is far more effective at affecting rheological properties. We reveal this behavior to be on account of a generalized scaling between the thickness of the adsorbed polymer layer and the observed yield stress reduction. As a result, electrosterically-based dispersants reduce the suspension's yield stress by nearly 10x at similar dosage as compared to electrostatic action alone. This nature of electrosteric effects allow for the formulation of suspensions wherein the critical solid loading, i.e., at which jamming is observed, to increase from 33 % for a Coulombic repulsion additive to 50 % (volume basis) for an electrosterically-based additive. By identifying the properties which result in the most effective dispersant, new insights are gained for the design of dispersants tailored for concentrated suspensions presenting strong charge screening behavior.

Keywords: *suspension rheology, aggregation, adsorption, dispersion, polymeric dispersant*

1. Introduction

The rheology of concentrated suspensions is of relevance to diverse industrial processes. Colloidal dispersions and gels exhibit a wide range of rheological properties such as aging, shear thickening/thinning, and yielding. In particular, the yield stress and viscosity of suspensions greatly affects the processing of materials for diverse applications including: cement and concrete pumping,[1,2] gel casting of ceramics,[3,4] drug delivery,[5,6] as well as in emerging technologies such as particulate flow batteries,[7,8] 3D-printing of slurries,[9,10] and more.[11,12] However, on account of their tendency to aggregate, the particles in a suspension may often organize into

flocs, and settle, resulting in undesirable behavior including a reduction of the (achievable) maximum solid volume fraction (ϕ_{max} = 0.35), and very high yield stress and viscosity that complicate slurry processing.[13,14]

Suspensions of strongly charged particles agglomerate especially readily in aqueous environments that present either a high ionic strength and/or a pH close to the particle's isoelectric point (IEP). In such suspensions, strong screening of electrostatic forces results in a sharp increase in yield stress with solid loading.[15] As a result, the maximum achievable particle loadings, i.e., prior to the onset of jamming are rather limited (ϕ_{max}). Polyelectrolytes (i.e., colloquially known as dispersants, or plasticizers) are often used to impart electrosteric barriers to particle aggregation, wherein formation of an adsorbed polymer layer limits the minimum distances of approach between particles, mitigating aggregation[16] Thus, such dispersants act to reduce the yield stress, while simultaneously enhancing the maximum particle loadings of dense suspensions. Polyelectrolytes can impart electrostatic repulsion and/or steric hindrance. Electrostatic interactions stem from the surface charges on bare particles and are altered by the adsorption of polyelectrolytes[17] Steric interactions are imparted by a physical barrier formed by the adsorbed polymers; this is often accomplished by grafting non-ionic side chains onto adsorbing polyelectrolytes to form 'comb' polyelectrolytes[18,19] The aqueous medium provides a good solvent for the side chains and they extend into the solution, preventing close approach of other particles. While commercially available dispersants are often effective in affecting suspension stability and rheology, considerable challenges remain. For example, it is difficult to design dispersants for

suspensions that self-regulate their pH, and that present high ionic strengths.[20] This is especially important in the event that the dispersant interacts with the solution resulting in aggregation mechanisms such as ion bridging interactions and/or complexation between polymers and multivalent counterions (e.g., Ca^{2+}).[21–23]

Portlandite (also known as slaked or hydrated lime or calcium hydroxide) is an example of a solid, which in suspension, self-regulates its pH (i.e., on account of its modest solubility; 20.3 mM at 25°C[24], I_m = 60.9 mM [molar ionic strength], and rapid dissolution behavior), and that presents a high-ionic strength and that is commonly used in applications including: water treatment[25–27], dental fillings[28–30], the food industry,[31,32] and as a building material.[33,34] On account of the relatively high-ionic strength resulting from its dissolution, portlandite presents weakly-charged, unstable nanosized particulates in suspension. This is problematic in applications where concentrated suspensions and good flow properties are required; as its tendency to aggregate and the low maximum solid volume fraction (ϕ_{max}) that is achievable make its processing difficult.[13] Therefore, this work seeks to elucidate the: (a) underlying mechanisms which control the aggregation of portlandite suspensions, (b) the interactions between commercial polymeric dispersants that present varying stabilization mechanisms (e.g., electrostatic, electrosteric, and mixed behavior) and $Ca(OH)_2$ suspensions. Special focus is paid to identify the characteristics of additives that would effectively improve the rheology of dense portlandite suspensions, and thereby offer guidelines for the design of new dispersants for new and established industrial applications.

2. Results and discussion

2.1 Aggregation, jamming and yielding of portlandite suspensions

Portlandite particles suspended in a self-saturated solution feature a zeta potential of +34 mV (Figure 1a). Typically, this magnitude of zeta potential would be large enough to impart electrostatic stability to a suspension.[35] However, electrostatic repulsion alone, is unable to prevent particle aggregation and produce stable suspensions of portlandite. As the suspensions approach their relatively low value of maximum achievable particle loading (ϕ_{max} = 0.35), yield stress sharply increases. Although this can occur in stable suspensions due to particle crowding from a heightened effective volume fraction because of long-range repulsive forces, the suspensions here have begun to visibly settle within 30 minutes of initial mixing. An examination of the interparticle interactions reveals the origin of this apparent inconsistency. The (symmetric) interparticle electric potential between portlandite particles as a function of distance from the particle surface *x* (Equation 1) includes the contributions of electrostatic repulsion (V_{es}) that can be modeled using the Hogg-Healy-Fuerstenau[36] solution to the Poisson-Boltzmann equation, and van der Waals attraction (V_{vdW}), calculated using nonretarded Hamaker pair potentials.[37,38]

$$V(x) = V_{es}(x) + V_{vdW}(x) = \pi\varepsilon_r\varepsilon_0\psi^2 R \ln(1 + \exp -\kappa x) - \frac{AR}{12x} \qquad \text{Eq. (1)}$$

Here, ε_r and ε_0 are the relative permittivity and permittivity of free space respectively, R is particle radius, κ is the inverse Debye length, x is distance from the particle surface. The surface potential ψ was estimated from the measured zeta potential (ζ) of the particles at the shear plane ($x_s \sim \kappa^{-1}$=1.1 nm)[39] as $\psi = \zeta \exp(\kappa x_s)$.

The Hamaker constant A = 2.2 × 10^{-20} J for $Ca(OH)_2$ was calculated following Lifshitz theory (see Section B, Equation S1 in SI).[40] The characteristic electrostatic decay length, or Debye length κ^{-1} is estimated as $\kappa^{-1} = \sqrt{2\varepsilon_r\varepsilon_0 kT/e^2 I}$, with k, T and e being the Boltzmann constant, temperature and the elementary charge, respectively, and I being the ionic strength of the medium that is written as $0.5\sum c_i z_i^2$ with c_i and z_i being the molar concentration and the valence of each ionic species present in the solution. For $Ca(OH)_2$ suspensions at their natural pH = 12.6, the ionic strength is 60.9 mM, resulting in a Debye length κ^{-1} = 1.2 nm.

Figure 1(a) shows the total interparticle interaction potentials as well as the contributions from electrostatic and van der Waals interactions. Strong screening of electrostatic interactions resulting from electric double layer (EDL) compression that arises from the high ionic strengths translates into electrostatic repulsion being effective only up to distances ≤ 5 nm across a range of particles sizes. The maximum repulsion occurs at a surface-to-surface separation around 0.7 nm, independent of particle size. The minimum energy of the repulsive barrier to prevent particle aggregation over a timescale τ can be estimated as $E_{min} = kT\ln(\tau f_c)$, with f_c being the collision frequency of particles under the influence of thermal forces (see Section C, SI).[40] The kinetic criterion to maintain suspension stability over 24 hours corresponds to E_{min} = 25 ± 3 *kT* for particles with a size on the order of 50 nm, 100 nm and 200 nm particles, as indicated by the horizontal dashed line in Figure 1(a). In general, for portlandite particles smaller than 65 nm, the strength of the repulsive potential was found to be smaller than the kinetic barrier across all interparticle separations while for particles larger than 65 nm, interparticle

repulsion was found to mitigate interparticle approach only up to distances smaller than around 3 nm. Therefore, although the measured zeta potential value of +34 mV at pH = 12.6 is relatively high, the high concentrations of counterions in the solution compress the EDL around the particles, thereby screening electrostatic repulsions very effectively. In consequence, the smaller primary portlandite particles are predicted to be unstable, and the larger particles are only stable at very small interparticle spacings. Therefore, the aggregation of portlandite particles for particle sizes < 200 nm is be expected. This results in an overall compromise in the suspension's stability.

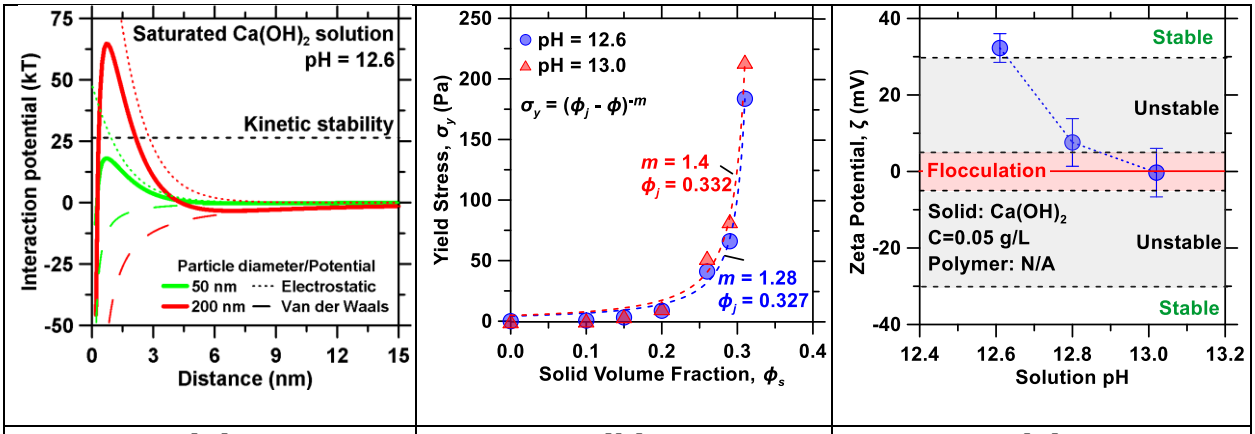

(a) **(b)** **(c)**

Figure 1: (a) The calculated interparticle potentials based on electrostatic and van der Waals interactions for $Ca(OH)_2$ particles in saturated $Ca(OH)_2$ solution (pH 12.6). **(b)** The yield stress as a function of solid volume fraction at varying pH in the absence of any dispersants. The data was fitted by a power-law function of the form $\sigma_y = (\phi_j - \phi)^m$. **(c)** The Zeta potential of $Ca(OH)_2$ particles as a function of pH in saturated $Ca(OH)_2$ solution with the pH adjusted using NaOH.

On account of their tendency to aggregate, and electrokinetic instability, portlandite suspensions display a sharp rise in their yield stress at moderate particle loadings (ϕ = 0.2) (Figure 1b). Therefore, an abnormally low maximum solid volume fraction ϕ_{max} = 0.35 (Figure 1c) is achievable; far inferior to the prediction for a monodisperse random close packing (ϕ_{rcp} = 0.638) configuration. These observations are consistent with previous reports on yielding and jamming behaviors of suspensions of aggregated particles. The yield stress (σ_y) of the suspension follows a power law scaling with particle volume fraction ($\sigma_y \sim \phi^m$), with $m \approx 5.75$, consistent with yield stress behavior of aggregating suspensions of mineral particles.[41]

Indeed, at their natural pH (12.6), portlandite suspensions are in the vicinity of their isoelectric point (IEP, pH_{IEP} = 13) (see Figure 1c). At the IEP, electrostatic interactions between the particles are entirely screened and only (attractive) van der Waals interactions operate. Consequently, the yield stress increases as particle aggregation is maximized. However, given the small pH gap that separates the native pH condition from the IEP, for portlandite suspensions, a negligible change in yielding behavior is observed vis-à-vis for suspensions regulated to their IEP. This indicates that particle aggregation is essentially maximized at pH 12.6. Significantly, these observations confirm that zeta potentials cannot be used as an indicator of stability for suspensions composed using strongly-charged particles that generate high-concentrations of solubilized counterions. It should be pointed out that changing (reducing) the solution pH to alter the zeta potential of the particles is ineffective for $Ca(OH)_2$ particulates; since on account of their solubility and

dissolution they self-regulate the pH of their local environment. It is especially for these reasons that dispersant-induced interactions are critical to control the rheology of portlandite (and other charged, soluble particle) suspensions.

3.2 Influence of dispersants on stability and rheology of portlandite suspensions

Polymeric dispersants are extensively used to reduce aggregation and promote particle dispersion for slurries composed of: ordinary portland cement,[19,42,43] titania,[44,45] and silicon nitride.[46] Such dispersants comprise linear polyelectrolyte backbones that carry ionizable groups that adsorb on the charged particle surfaces even in high ionic strength conditions. High charge density, low-entropy and large flexibility and conformability of the polyelectrolyte contribute towards lowering of the total free energy of the system upon adsorption, promoting the polyelectrolytes to form an adsorbed layer on the particle surfaces with sections of the chain adsorbed on the surfaces and other sections forming loops and tails that hang off the particle surfaces; thereby extending into solution. These loops and tails provide a strong steric repulsion and offer resistance to compression and thus provide an extra repulsive contribution to interparticle interactions.[19,42] The length scale and strength of these electrosteric repulsions depends on the thickness of the adsorbed layer, which in turn is dictated by the length, charge density and stiffness of the polyelectrolyte chain as well as the strength of the attractive electrostatic interactions between the polyelectrolyte and the particles.[17,43,46]

Figure 2 elaborates the effects of three dispersants — a polyacrylic acid-based linear polyelectrolyte dispersant (PAA), a lignosulfonate dispersant (LS), and a polycarboxylate ether-based comb polyelectrolyte dispersant composed of a polyacrylic acid backbone and polyethylene glycol sidechains (PCE) — on the propensity for aggregation and yielding behavior of $Ca(OH)_2$ suspensions. In general, the PCE dispersant dramatically reduced both the since of aggregates formed, and the rate of their formation as compared to the other dispersants (see Figure 3a). The mean aggregate increased roughly linearly with the square root of time following the relationship, $a_z = At^{0.5}$, indicating the importance of diffusion-controlled aggregation. The parameter *A* describes the rate of aggregation and the values of which (A_{none} = 1189, A_{LS} = 857, A_{PAA} = 299, and A_{PCE} = 191) corresponded with the effectiveness of each dispersant in reducing aggregation in the suspensions.

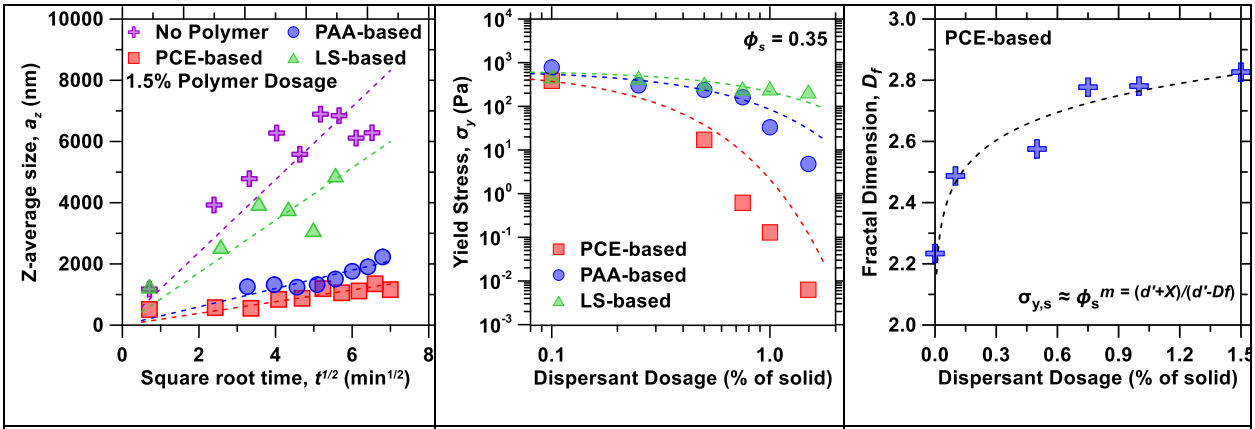

Figure 2: (a) The "Z-average" size (determined by the method of cumulants as interpretation of DLS data) of $Ca(OH)_2$ aggregates as determined by DLS in suspensions composed at ϕ = 0.002. These values are indicative of floc size - as

$Ca(OH)_2$ particles aggregate, the z-average size increases. The lines indicate fits of the form $a_z = At^{0.5}$ to the data, where *A* and *B* were fitting parameters. The yield stress of $Ca(OH)_2$ suspensions as a function of: **(b)** Dispersant dosage for the three types of dispersants at ϕ = 0.35. The dashed lines in (b) indicate exponential function fits to the data of the form $\sigma_y = Aexp^{Bx}$. **(c)** Fractal dimension calculated from power-law scaling of yield stress vs. solid volume fraction for PCE dispersant.

Expectedly, reduced aggregation and smaller aggregate sizes result in suspensions that show a smaller yield stress upon the addition of a dispersant. For example, at a constant solid volume fraction (ϕ = 0.35), significant reductions in the yield stress were observed with increasing polymer dosages (Figure 2b). A remarkable 10^5-fold decrease in yield stress was achieved at a PCE dosage 1.5 mass % (polymer/solid). The reduction of the yield stress as a function of dispersant dosage follow an exponential dependence of the form $\sigma_y = Aexp^{Bx}$ where A = 663 Pa (the yield stress of a suspension made without polymer) and B varies with the dispersant used (B_{PCE} = -5.74 far exceeds B_{PAA} = -2.06 and B_{LS} = -1.13). On account of the superior dispersion action of the PCE, its effects on yielding behavior were examined over a wider range of volume fractions (see Figure S2, SI). Prominently, beyond a consistent reduction in the yield stress with dispersant dosage, at a fixed PCE dosage, e.g., 1.5 mass % of particles, the maximum achievable particle volume fraction increased by 1.5x from 0.33 to 0.50; i.e., corresponding to a significant increase in the particle density per unit volume. This is reflected in a significant increase in the fractal dimension of the suspensions made with higher dosages of

PCE. The fractal dimension D_f, extracted from a power-law fit of yield stress vs. solid volume fraction of the form $\sigma_y \sim \phi_s^{\,m}$ where $m = \frac{d'+X}{d'-D_f}$, d' being the number of spatial dimensions (3) and X as the fractal dimension of the cluster backbones, taken as 1 (see Figure 2c).[47] As the value of the fractal dimensions approaches 3, the individual flocs are packed in a more dense arrangement, allowing for increased maximum particle volume fraction.

To gain further insights into actions of the different dispersants their adsorption on portlandite surfaces was examined. The amount adsorbed, Γ, was fit to a Langmuir isotherm (see Figure 3b) that is written as $\frac{c_{free}}{\Gamma} = \frac{c_{free}}{\Gamma_{max}} + \frac{1}{\Gamma_{max}K}$.[48,49] This equation shows a plateau in the amount adsorbed (Γ_{max}) as a function of the non-adsorbed (free) dispersant concentration (c_{free}) and features a fitting parameter K which describes the ease and tendency of polymer adsorption. It should be noted that adsorption behavior was only examined in a range that is expected to be relevant for typical applications, i.e., ≤ 5 mass % dispersant by mass of solid [N.B.: It is important to limit the dispersant dosages to restrict the abundance of free polymer in solution, which could induce attractive depletion forces]. An assumption of the Langmuir analysis suggests *on-average* monolayer adsorption; an assessment which is expected to be reasonable for the dosages considered herein although multilayer adsorption may occur at yet higher dispersant concentrations.[17,19,50] Analysis of the adsorption isotherms indicates that although LS dispersants may be expected to show greater adsorption than PAA or PCE, i.e., due to the higher affinity of the particle surfaces for sulfonate groups as compared to carboxylate groups, PAA adsorbs far more readily, especially at low dispersant dosages. This

behavior which is reflected by the binding affinity *K* of a given dispersant (Table 1) is thought to be on account of the aromatic rings within the LS dispersant's structure which reduces the flexibility of polymer chains thereby entropically limiting adsorption due to the lack of favorable conformations that are accessible. On the other hand, the adsorption behavior of the PCE reflects its reduced volumetric charge density, and the physical interference caused by its dangling side-chains which hinder its adsorption. On the other hand, the lack of dense side-chains for the PAA dispersant resulted in the adsorbed conformation of loops and tails, providing some steric exclusion to the particles while retaining high adsorption.

When the yield stress data for each dispersant is plotted against the amount of adsorbed dispersant (Figure 3c) it provides an indication of the efficacy of each dispersant, i.e., in terms of their ability to induce yield stress reductions (see Figure 3b). When normalized by adsorbed dispersant, it noted that the PCE is the most effective dispersant. In effect, while the PAA and LS dispersants show similar behavior at low levels of adsorption; LS shows a saturation in affecting yielding behavior while the PAA dispersant in fact improves its effectiveness above an adsorption level around 0.08 $g_{polymer}/g_{solid}$, Significantly, however, there is a marked difference in the effectiveness of the dispersants, with the PCE showing clearly superior performance.

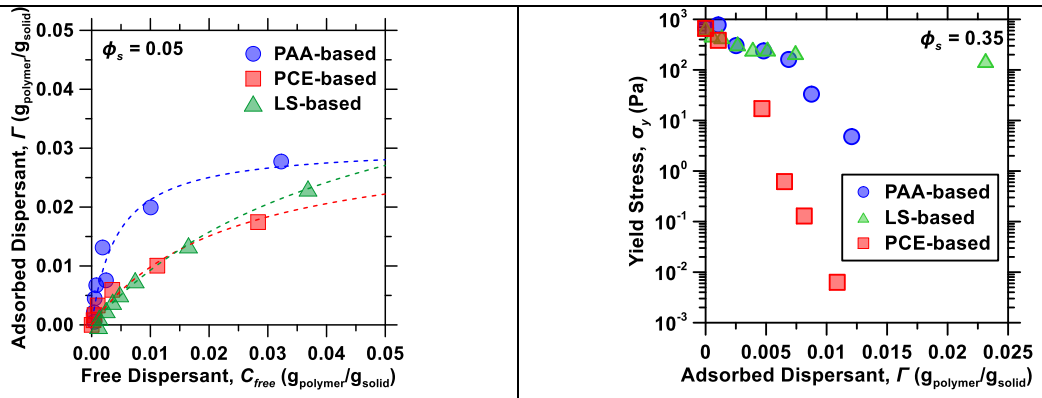

(a) **(b)**

Figure 3: (a) The amount of dispersant adsorbed to particles surfaces as a function of the free dispersant concentration in solution. The data is fit to a Langmuir expression for monolayer adsorption (dashed lines). **(b)** The yield stress of portlandite suspensions as a function of the amount of dispersant adsorbed on the particle surfaces.

To assess the effects of the dispersants on altering interparticle separations, to a first approximation, the average surface-to-surface separation amongst the particles was assessed using information of the solid volume fraction in the suspension, and the particle size distribution (i.e., from the number density of particles per unit volume; see SI, Section C). Figure 4(a) shows a simplified trace of a neat portlandite suspension's yield stress as a function of the interparticle spacing for a range of volume fractions; $0.10 \leq \varphi_s \leq 0.35$. This relationship creates a basis, although greatly simplified, to establish how the change in the yield stress ($\Delta\sigma_y$) produced by addition of a dispersant is correlated with a change (increase) in the average interparticle spacing (Δx). The outcomes of this analysis which are shown in Figure 4(b) indicate that, in effect, the differing ability of the dispersants to

reduce the suspension's yield stress are intrinsically related to their ability to induce controllable separations between particles as a function of their adsorption behavior. Since, in effect, such separation ability is a function of dominantly electrosteric behavior – in high ionic strength suspensions – a relevant indicative dispersant attribute for a given dispersant is its hydrodynamic radius (r_H, see Table 1).

Table 1: Select data for each dispersant as determined by GPC (M_w), DLS (r_H), and TOC (Γ_{max} and K).

Dispersant Type	**Mass-average molecular weight, M_w (g/mol)**	**Hydrodynamic radius, r_H (nm)**	**Adsorption capacity, Γ_{max} (g_{poly}/g_{solid})**	**Binding affinity, K (~)**
PCE	39,467	11.34	0.0325	43.32
PAA	6,092	4.45	0.0305	229.7
LS	4,050	2.61	0.0520	21.75

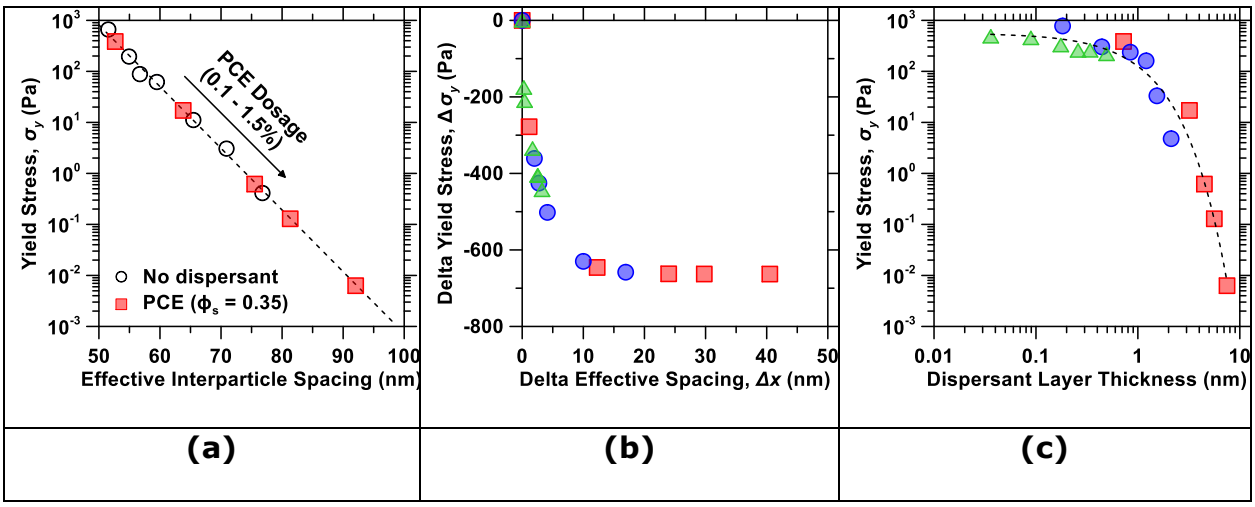

(a) **(b)** **(c)**

Figure 4: (a) The suspension's yield stress as a function of interparticle (surface-to-surface) separation for a neat portlandite suspension. By mapping the measured yield stress to the interparticle spacing – the effect of a given dispersant on reducing the yield stress at a specific dosage can be established. **(b)** Continuation of analysis in **(a)** showing the reduction in yield stress as the effective interparticle spacing increases; the yield stress can be reduced to a negligible value with approximately +10 nm of effective interparticle spacing. **(c)** The yield stress as a function of an effective dispersant layer thickness for all the polymers examined herein. The data collapses on a single curve that is expressed as: $\sigma_y = Aexp^{Bx}$. In general, it is seen that the yield stress reduces by nearly 5 orders of magnitude when the dispersant layer thickness exceeds the electrostatic screening length.

The hydrodynamic radius describes the physical size of the polymer molecule in a suspension. Although r_H does not perfectly describe the size of the conformation of the adsorbed polymer, it offers an estimate of the interaction distance for steric repulsion of each dispersant. Thus, the effectiveness of each dispersant, i.e., the dispersant layer thickness, can be described by the product of its fractional amount adsorbed (i.e., surface coverage, m = Γ/Γ_{max}) and its hydrodynamic radius (see Figure 4c). Remarkably, for a monophasic solid, it is observed that the yielding behavior of its suspensions are generally correlated with the dispersant layer thickness – for dispersants which feature dominantly electrostatic and/or electrosteric attributes. In addition, it is noted that sharp reductions – nearly around 5 orders of magnitude – in the yield stress are indeed produced when the

dispersant layer thickness, exceeds the electrostatic screening length (i.e., Debye length, κ^{-1}). This observation indicates that, in general, the most prominent attribute of a dispersant is to offer a sufficient adsorbed thickness that induces physical separation amongst particles over a length scale greater than that over which Coulombic forces would operate. Of course, the interparticle interactions produced by adsorbed polymers are controlled by their structure. As such, since the LS and PAA dispersants do not feature branched or grafted side chains; they are not expected to provide significant steric repulsion. The presence of the side chains reduces the influence of electrostatic repulsion, as the distribution of charge in the electric double layer decays strongly with distance. Taken together, since the PCE is the only dispersant examined herein that is capable of producing a substantial adsorbed layer thickness and thus steric repulsion, it is the dispersant that is, in turn, most effective at creating larger particle separations.

4. Summary and conclusions

Dispersants to be used in concentrated suspensions at high ionic strengths should be tailored to maximize the impact of steric repulsion. High ionic strengths disrupt electrostatic repulsion by screening charge and favor aggregating effects such as ion bridging. Steric repulsion is not affected by these issues, and provides stronger, more consistent effectiveness. PCE, a polymeric dispersant used in the cement industry, was found to provide strong steric repulsion for heavily aggregating suspensions of calcium hydroxide, reducing yield stress and viscosity and increasing maximum solid volume fraction. Simple guidelines for the engineering and improvement of polymeric dispersants were provided, including hypotheses for

targeted functionalization and polymer selection. Further research is required to test these insights and expand these investigations to suspensions containing other solids and solution chemistries. The information gained from this investigation can be used to produce dispersants which are designed with specific applications in mind, enabling greater control over rheology and higher process efficiencies.

5. Materials and Methods

5.1. Materials and sample preparation

Commercially-available portlandite ($Ca(OH)_2$; Standard Hydrated Lime, Mississippi Lime Company) was used. It featured a purity of 94 % ± 2 % (by mass) with the remainder being composed of $CaCO_3$ as determined by thermogravimetric analysis (TGA; STA 6000, Perkin Elmer). The particle size distribution of the portlandite was measured using static light scattering (SLS; LS13-320, Beckman Coulter), using a refractive index of 1.574 + 0.000*i*.[51] The particulates was dispersed using ultrasonication in isopropanol (IPA) which was used as the carrier fluid. The median particle diameter (d_{50}) of the particulates was estimated as 3.8 μm ± 0.2 μm (Figure 5a). The density of the particulates was measured as 2235 kg/m^3 using helium pycnometry (AccuPyc II 1340, Micromeritics).

The morphology of the ulatesparticles was examined using a field emission-scanning electron microscope using energy dispersive X-ray spectroscopy (SEM-EDS; FEI NanoSEM 230). All SEM micrographs were acquired in secondary electron mode with a spot size of 4.0 nm, at an accelerating voltage of 10 kV, and a working

distance of ≈ 5.5 mm. As shown in Figure 5(b), the particles form aggregates which are of similar size as is measured by static light scattering.

Since light scattering is known to be ineffective in determining the primary particle size of the aggregated portlandite particulates, [13,33] transmission electron microscopy (TEM; FEI T12 Quick CryoEM and CryoET) was used to examine the primary particle size. A dilute suspension of portlandite particulates dispersed in IPA was deposited on to a TEM grid; and the solvent was evaporated thereafter. Although large aggregates were still observed, the primary particle size was established as being on the order of 20-to-200 nm (Figure 5c), as suggested previously.[13,33,34] However, it was not possible to meaningfully, from a statistical basis, resolve a sufficient number of unagglomerated particles to establish a particle size distribution from the TEM imaging.

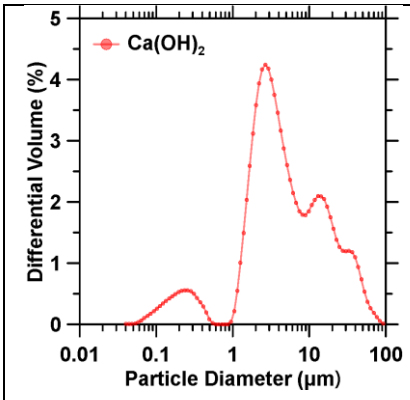

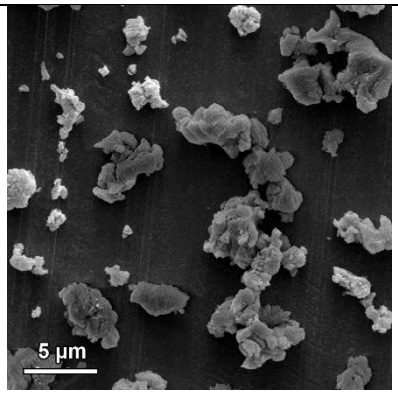

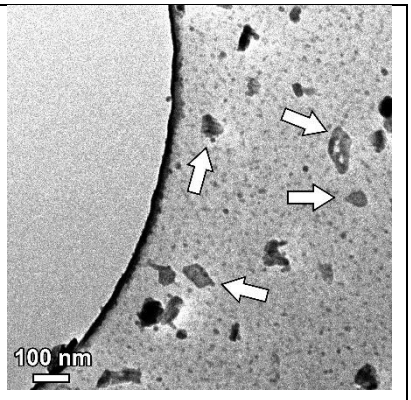

(a) | **(b)** | **(c)**

Figure 5: (a) The particle size distribution of portlandite particulates as determined by static light scattering (SLS), revealing a volumetric median diameter, d_{50} = 3.8 μm. **(b)** A SEM micrograph displaying the morphology of

portlandite particle aggregates. **(c)** A TEM micrograph of portlandite particulates with primary particles indicated by the arrows.

Three commercially available dispersants were used including: (1) a polyacrylic acid-based dispersant (PAA, Acumer 9000, Dow Chemical), (2) a lignosulfonate-based dispersant (LS, MasterPolyheed 997, BASF Corporation), and (3) a poly carboxylate ether-based dispersant (PCE, MasterGlenium 7500, BASF Corporation). The functional groups present in each polymer were qualitatively determined (see Figure S1 in SI) using Fourier transform infrared spectroscopy (FTIR; PerkinElmer Spectrum Two). In brief, LS contains sulfonic acid groups,[52] PAA presents carbonyl groups, and PCE presents carbonyl groups associated with its PAA backbone and ether groups corresponding to its polyethylene glycol (PEG) side chains [N.B.: the ratio between the abundance between carbonyl:ether groups is on the order of 0.09:1 on a mass basis].[46] The solids content of each additive was determined as 44.9 mass %, 49.8 mass %, and 25.6 mass %, respectively, by gravimetric analysis. The dispersants were dosed at a level ranging between 0-to-1.5 mass % of the solid content in the suspension, considering the solids content of the polymer dispersant.

In order to prevent any complications caused by the dissolution of portlandite, a previously saturated, filtered saturated $Ca(OH)_2$ solution were used as the suspending fluid. The saturated $Ca(OH)_2$ solution was prepared by adding excess portlandite to deionized (DI) water, allowing for the solids to settle, and then filtering the solution using a 0.20 μm syringe filter. To produce suspensions,

polymeric dispersants (when used) were added to the saturated $Ca(OH)_2$ solution, and then solid portlandite particulates were added to the solution. The mixture was first mixed by hand, and then stirred for 120 s using a four-blade impeller-type high-shear mixer (RW 20 Digital, IKA) at 500 rpm to produce a well-dispersed, homogenous suspension.

5.2. Experimental methods

5.2.1. Characterization of polymers

Molecular weight determination: The molecular weight of each dispersant was measured by gel permeation chromatography (GPC; Waters Alliance HPLC System, 2695 Separation Module) with a two-column setup (Toso TSKgel G3000PWXL and TSKgel G5000PWXL), with two detectors, one to determine the differential refractive index (dRI; Waters 2414 Differential Refractometer) and an optical detector (Waters 2998 Photodiode Array Detector). The solvent used was deionized (MilliQ) water with 10 mM NaH_2PO_4 and 1.5 mM NaN_3 present, to buffer the solution to pH 7. The flow rate of the instrument was set to 1 mL/min, with an injection volume of 100 µL.

Dynamic light scattering: To assess the hydrodynamic radius (r_h, nm) of the polymers present in each of the three dispersants, dynamic light scattering (DLS) analysis (Malvern, Zetasizer Nano) was carried out. Each sample was diluted by addition of deionized (MilliQ) water (0.05 $g_{solids}/L_{solution}$) and the Z-average size of

particle aggregates was determined by cumulants analysis (Malvern, Zetasizer Software).

5.2.2. Characterization of portlandite ($Ca(OH)_2$) suspensions

Zeta potential: To assess the electrokinetic interactions in the suspensions, the zeta potential (ζ, mV) was determined by measurement of electrophoretic mobilities using Phase Analysis Light Scattering (ZetaPALS, Brookhaven Instruments Corporation). The measurements were carried out on dilute portlandite suspensions (0.05 $g_{solids}/L_{solution}$) for a variety of dispersant types and dosages. In addition, in select circumstances the pH of the suspensions was adjusted to 12.8 and 13.0 by the addition of sodium hydroxide (NaOH).

Suspension rheology: The rheological behavior of portlandite suspensions was assessed for a range of particle volume fractions and dispersant dosages using a combined motor-transducer rheometer (DHR-2, TA Instruments). For all measurements, the suspensions were conditioned to a temperature of 25 ± 0.1 °C. Two types of analyses were carried out:

- The yield stress (σ_y) and shear rate ($\dot{\gamma}$)-dependent viscosity (η) were determined via a shear rate sweep. Before the sweep, a 60 s pre-shear at $\dot{\gamma} = 100\ s^{-1}$ was performed to remove any shear history effects. An ascending sweep was imposed in logarithmically spaced steps (5 points per decade) from $\dot{\gamma} = 1 \times 10^{-3}\ s^{-1}$ to $200\ s^{-1}$ with a 10 s data-averaging period. The ascending sweep was followed by a descending sweep over the same shear rate range.

- The viscoelastic behavior and strength (elasticity) of aggregates in the suspensions were characterized via small amplitude oscillatory (SAOS) rheometry. Following the shear flow experiment, a shear-strain amplitude (γ_A) sweep from γ_A = 0.001% to 400% was performed, at a fixed frequency of 1 Hz.

Polymer adsorption: The extent of polymer adsorption onto portlandite surfaces was determined by use of a total organic carbon (TOC) analyzer (Shimadzu, TOC-L). Here, suspensions of $\varphi = 0.05$ with varying dispersant contents up to 5 % by mass of solids (i.e., an upper bound on dosage for typical applications) were composed and allowed to equilibrate for 24 hours. Following such equilibration, the suspensions were then centrifuged for 15 minutes at 4696 rpm, and the supernatant was removed and filtered using a 0.20 μm syringe filter. With all solid particles removed, the amount of non-adsorbed polymer present therein was measured via TOC analysis. As the inorganic carbon content may be elevated due to the formation of calcium carbonate ($CaCO_3$), a non-purgeable organic carbon (NPOC) analysis was performed. Since the carbon content of each of the dispersants was unknown, a calibration for each of the three dispersants was also established by testing a series of known dilutions of dispersant up to a maximum dosage equivalent to that found in the adsorption experiments. This allowed for a direct conversion to be made between the NPOC content and dispersant dosage, which was unique for each dispersant. The extent of polymer adsorption was then calculated using a mass balance with the original amount of polymer added.

Dynamic light scattering: To assess aggregation kinetics of suspensions for varying dispersant types and dosages, dynamic light scattering (DLS) analysis (Malvern, Zetasizer Nano) was carried out over time. Using highly diluted suspensions (0.05 $g_{solids}/L_{solution}$), the Z-average size of particle aggregates was determined by cumulants analysis (Malvern, Zetasizer Software). Each measurement was taken at approximately 5-minute intervals for up to 1 hour. Individual measurements took around 2 minutes each.

6. Acknowledgements

The authors acknowledge financial support for this research from the National Science Foundation (DMREF: 1922167, CMMI: 1562066, CAREER: 1253269), Department of Energy: Office of Fossil Energy via the National Energy Technology Laboratory (NETL; DE-FE0029825 and DE-FE0031718), The Anthony and Jeanne Pritzker Family Foundation, and TRANSCEND: A joint UCLA-NIST Consortium that is funded by its industry and agency partners. This research was conducted in the Laboratory for the Chemistry of Construction Materials (LC^2) and the Electron Microscopy Core Facility at UCLA. The authors gratefully acknowledge the support provided by these laboratories. The contents of this paper reflect the views and opinions of the authors, who are responsible for the accuracy of the datasets presented herein, and do not reflect the views and/or policies of the funding agencies, nor do the contents constitute a specification, standard or regulation.

7. References

(1) Roussel, N. *Understanding the Rheology of Concrete*; Elsevier, 2011.

(2) Banfill, P. F. G. The Rheology of Fresh Cement and Concrete - A Review; 2003.

(3) Liu, X.; Huang, Y.; Yang, J. Effect of Rheological Properties of the Suspension on the Mechanical Strength of Al2O3–ZrO2 Composites Prepared by Gelcasting. *Ceramics International* **2002**, *28* (2), 159–164. https://doi.org/10.1016/S0272-8842(01)00072-4.

(4) Johnson, S. B.; Dunstan, D. E.; Franks, G. V. Rheology of Cross-Linked Chitosan–Alumina Suspensions Used for a New Gelcasting Process. *Journal of the American Ceramic Society* **2002**, *85* (7), 1699–1705. https://doi.org/10.1111/j.1151-2916.2002.tb00338.x.

(5) Vintiloiu, A.; Leroux, J.-C. Organogels and Their Use in Drug Delivery — A Review. *Journal of Controlled Release* **2008**, *125* (3), 179–192. https://doi.org/10.1016/j.jconrel.2007.09.014.

(6) Zignani, M.; Tabatabay, C.; Gurny, R. Topical Semi-Solid Drug Delivery: Kinetics and Tolerance of Ophthalmic Hydrogels. *Advanced Drug Delivery Reviews* **1995**, *16* (1), 51–60. https://doi.org/10.1016/0169-409X(95)00015-Y.

(7) Bauer, W.; Nötzel, D. Rheological Properties and Stability of NMP Based Cathode Slurries for Lithium Ion Batteries. *Ceramics International* **2014**, *40* (3), 4591–4598. https://doi.org/10.1016/j.ceramint.2013.08.137.

(8) Mubeen, S.; Jun, Y.; Lee, J.; McFarland, E. W. Solid Suspension Flow Batteries Using Earth Abundant Materials. *ACS Appl. Mater. Interfaces* **2016**, *8* (3), 1759–1765. https://doi.org/10.1021/acsami.5b09515.

(9) Lowke, D.; Dini, E.; Perrot, A.; Weger, D.; Gehlen, C.; Dillenburger, B. Particle-Bed 3D Printing in Concrete Construction – Possibilities and Challenges. *Cement and Concrete Research* **2018**, *112*, 50–65. https://doi.org/10.1016/j.cemconres.2018.05.018.

(10) Ren, X.; Shao, H.; Lin, T.; Zheng, H. 3D Gel-Printing—An Additive Manufacturing Method for Producing Complex Shape Parts. *Materials & Design* **2016**, *101*, 80–87. https://doi.org/10.1016/j.matdes.2016.03.152.

(11) Gaborski, T. R.; Snyder, J. L.; Striemer, C. C.; Fang, D. Z.; Hoffman, M.; Fauchet, P. M.; McGrath, J. L. High-Performance Separation of Nanoparticles

with Ultrathin Porous Nanocrystalline Silicon Membranes. *ACS Nano* **2010**, *4* (11), 6973–6981. https://doi.org/10.1021/nn102064c.

(12) Houst, Y. F.; Bowen, P.; Perche, F.; Kauppi, A.; Borget, P.; Galmiche, L.; Le Meins, J.-F.; Lafuma, F.; Flatt, R. J.; Schober, I.; et al. Design and Function of Novel Superplasticizers for More Durable High Performance Concrete (Superplast Project). *Cement and Concrete Research* **2008**, *38* (10), 1197–1209. https://doi.org/10.1016/j.cemconres.2008.04.007.

(13) Ruiz-Agudo, E.; Rodriguez-Navarro, C. Microstructure and Rheology of Lime Putty. *Langmuir* **2010**, *26* (6), 3868–3877. https://doi.org/10.1021/la903430z.

(14) Fourmentin, M.; Ovarlez, G.; Faure, P.; Peter, U.; Lesueur, D.; Daviller, D.; Coussot, P. Rheology of Lime Paste—a Comparison with Cement Paste. *Rheol Acta* **2015**, *54* (7), 647–656. https://doi.org/10.1007/s00397-015-0858-7.

(15) Leong, Y.; Boger, D. V.; Parris, D. Surface Chemistry and Rheological Properties of Zirconia Suspensions. *Journal of Rheology* **1991**, *35* (1), 149–165. https://doi.org/10.1122/1.550225.

(16) F. Luckham, P.; Klein, J. Forces between Mica Surfaces Bearing Adsorbed Polyelectrolyte, Poly- L -Lysine, in Aqueous Media. *Journal of the Chemical Society, Faraday Transactions 1: Physical Chemistry in Condensed Phases* **1984**, *80* (4), 865–878. https://doi.org/10.1039/F19848000865.

(17) Zingg, A.; Winnefeld, F.; Holzer, L.; Pakusch, J.; Becker, S.; Gauckler, L. Adsorption of Polyelectrolytes and Its Influence on the Rheology, Zeta Potential, and Microstructure of Various Cement and Hydrate Phases. *Journal of Colloid and Interface Science* **2008**, *323* (2), 301–312. https://doi.org/10.1016/j.jcis.2008.04.052.

(18) De Hazan, Y.; Heinecke, J.; Weber, A.; Graule, T. High Solids Loading Ceramic Colloidal Dispersions in UV Curable Media via Comb-Polyelectrolyte Surfactants. *Journal of Colloid and Interface Science* **2009**, *337* (1), 66–74. https://doi.org/10.1016/j.jcis.2009.05.012.

(19) Kirby, G. H.; Lewis, J. A. Comb Polymer Architecture Effects on the Rheological Property Evolution of Concentrated Cement Suspensions. *Journal of the American Ceramic Society* **2004**, *87* (9), 1643–1652. https://doi.org/10.1111/j.1551-2916.2004.01643.x.

(20) Dean, S.; Chen, C.-T.; Struble, L.; Zhang, H. Using Dynamic Rheology to Measure Cement-Admixture Interactions. *J. ASTM Int.* **2006**, *3* (3), 12787. https://doi.org/10.1520/JAI12787.

(21) Mirnezami, M.; Restrepo, L.; Finch, J. A. Aggregation of Sphalerite: Role of Zinc Ions. *Journal of Colloid and Interface Science* **2003**, *259* (1), 36–42. https://doi.org/10.1016/S0021-9797(02)00101-7.

(22) Sowoidnich, T.; Rachowski, T.; Rößler, C.; Völkel, A.; Ludwig, H.-M. Calcium Complexation and Cluster Formation as Principal Modes of Action of Polymers Used as Superplasticizer in Cement Systems. *Cement and Concrete Research* **2015**, *73*, 42–50. https://doi.org/10.1016/j.cemconres.2015.01.016.

(23) Plank, J.; Sachsenhauser, B. Experimental Determination of the Effective Anionic Charge Density of Polycarboxylate Superplasticizers in Cement Pore Solution. *Cement and Concrete Research* **2009**, *39* (1), 1–5. https://doi.org/10.1016/j.cemconres.2008.09.001.

(24) Bates, R. G.; Bower, V. E.; Smith, E. R. Calcium Hydroxide as a Highly Alkaline PH Standard; 1956. https://doi.org/10.6028/jres.056.040.

(25) Murphy, T. P.; Prepas, E. E.; Lim, J. T.; Crosby, J. M.; Walty, D. T. Evaluation of Calcium Carbonate and Calcium Hydroxide Treatments of Prairie Drinking Water Dugouts. *Lake and Reservoir Management* **1990**, *6* (1), 101–108. https://doi.org/10.1080/07438149009354700.

(26) Lim, S.; Jeon, W.; Lee, J.; Lee, K.; Kim, N. Engineering Properties of Water/Wastewater-Treatment Sludge Modified by Hydrated Lime, Fly Ash and Loess. *Water Research* **2002**, *36* (17), 4177–4184. https://doi.org/10.1016/S0043-1354(02)00150-1.

(27) Chen, Q.; Luo, Z.; Hills, C.; Xue, G.; Tyrer, M. Precipitation of Heavy Metals from Wastewater Using Simulated Flue Gas: Sequent Additions of Fly Ash, Lime and Carbon Dioxide. *Water Research* **2009**, *43* (10), 2605–2614. https://doi.org/10.1016/j.watres.2009.03.007.

(28) Rosenberg, B.; Murray, P. E.; Namerow, K. The Effect of Calcium Hydroxide Root Filling on Dentin Fracture Strength. *Dental Traumatology* **2007**, *23* (1), 26–29. https://doi.org/10.1111/j.1600-9657.2006.00453.x.

(29) Sathorn, C.; Parashos, P.; Messer, H. Antibacterial Efficacy of Calcium Hydroxide Intracanal Dressing: A Systematic Review and Meta-Analysis. *International Endodontic Journal* **2007**, *40* (1), 2–10. https://doi.org/10.1111/j.1365-2591.2006.01197.x.

(30) SJöGREN, U.; Figdor, D.; Spångberg, L.; Sundqvist, G. The Antimicrobial Effect of Calcium Hydroxide as a Short-Term Intracanal Dressing. *International Endodontic Journal* **1991**, *24* (3), 119–125. https://doi.org/10.1111/j.1365-2591.1991.tb00117.x.

(31) Martínez-Bustos, F.; Chang, Y. K.; Bannwart, A. C.; Rodríguez, M. E.; Guedes, P. A.; Gaiotti, E. R. Effects of Calcium Hydroxide and Processing Conditions on Corn Meal Extrudates. *Cereal Chemistry* **1998**, *75* (6), 796–801. https://doi.org/10.1094/CCHEM.1998.75.6.796.

(32) Han, L.; Lu, Z.; Hao, X.; Cheng, Y.; Li, L. Impact of Calcium Hydroxide on the Textural Properties of Buckwheat Noodles. *Journal of Texture Studies* **2012**, *43* (3), 227–234. https://doi.org/10.1111/j.1745-4603.2011.00331.x.

(33) Rodriguez-Navarro, C.; Hansen, E.; Ginell, W. S. Calcium Hydroxide Crystal Evolution upon Aging of Lime Putty. *Journal of the American Ceramic Society* **1998**, *81* (11), 3032–3034. https://doi.org/10.1111/j.1151-2916.1998.tb02735.x.

(34) Cazalla, O.; Rodriguez-Navarro, C.; Sebastian, E.; Cultrone, G.; Torre, M. J. D. la. Aging of Lime Putty: Effects on Traditional Lime Mortar Carbonation. *Journal of the American Ceramic Society* **2000**, *83* (5), 1070–1076. https://doi.org/10.1111/j.1151-2916.2000.tb01332.x.

(35) Wiśniewska, M. Influences of Polyacrylic Acid Adsorption and Temperature on the Alumina Suspension Stability. *Powder Technology* **2010**, *198* (2), 258–266. https://doi.org/10.1016/j.powtec.2009.11.016.

(36) Hogg, R.; W. Healy, T.; W. Fuerstenau, D. Mutual Coagulation of Colloidal Dispersions. *Transactions of the Faraday Society* **1966**, *62* (0), 1638–1651. https://doi.org/10.1039/TF9666201638.

(37) Hamaker, H. C. The London—van Der Waals Attraction between Spherical Particles. *Physica* **1937**, *4* (10), 1058–1072. https://doi.org/10.1016/S0031-8914(37)80203-7.

(38) Aschauer, U.; Burgos-Montes, O.; Moreno, R.; Bowen, P. Hamaker 2: A Toolkit for the Calculation of Particle Interactions and Suspension Stability and Its Application to Mullite Synthesis by Colloidal Methods. *Journal of Dispersion Science and Technology* **2011**, *32* (4), 470–479. https://doi.org/10.1080/01932691003756738.

(39) Ding, W.; Liu, X.; Song, L.; Li, Q.; Zhu, Q.; Zhu, H.; Hu, F.; Luo, Y.; Zhu, L.; Li, H. An Approach to Estimate the Position of the Shear Plane for Colloidal

Particles in an Electrophoresis Experiment. *Surface Science* **2015**, *632*, 50–59. https://doi.org/10.1016/j.susc.2014.08.024.

(40) Israelachvili, J. N. *Intermolecular and Surface Forces*; Academic Press, 2015.

(41) Boger, D. V. Rheology of Slurries and Environmental Impacts in the Mining Industry. *Annual Review of Chemical and Biomolecular Engineering* **2013**, *4* (1), 239–257. https://doi.org/10.1146/annurev-chembioeng-061312-103347.

(42) Lewis, J. A. Colloidal Processing of Ceramics. *Journal of the American Ceramic Society* **2000**, *83* (10), 2341–2359. https://doi.org/10.1111/j.1151-2916.2000.tb01560.x.

(43) Winnefeld, F.; Becker, S.; Pakusch, J.; Götz, T. Effects of the Molecular Architecture of Comb-Shaped Superplasticizers on Their Performance in Cementitious Systems. *Cement and Concrete Composites* **2007**, *29* (4), 251–262. https://doi.org/10.1016/j.cemconcomp.2006.12.006.

(44) Morris, G. E.; Skinner, W. A.; Self, P. G.; Smart, R. St. C. Surface Chemistry and Rheological Behaviour of Titania Pigment Suspensions. *Colloids and Surfaces A: Physicochemical and Engineering Aspects* **1999**, *155* (1), 27–41. https://doi.org/10.1016/S0927-7757(98)00631-1.

(45) Farrokhpay, S. A Review of Polymeric Dispersant Stabilisation of Titania Pigment. *Advances in Colloid and Interface Science* **2009**, *151* (1), 24–32. https://doi.org/10.1016/j.cis.2009.07.004.

(46) Rueschhoff, L. M.; Youngblood, J. P.; Trice, R. W. Stabilizing Highly Loaded Silicon Nitride Aqueous Suspensions Using Comb Polymer Concrete Superplasticizers. *Journal of the American Ceramic Society* **2016**, *99* (12), 3857–3865. https://doi.org/10.1111/jace.14432.

(47) Shih, W.-H.; Shih, W. Y.; Kim, S.-I.; Liu, J.; Aksay, I. A. Scaling Behavior of the Elastic Properties of Colloidal Gels. *Phys. Rev. A* **1990**, *42* (8), 4772–4779. https://doi.org/10.1103/PhysRevA.42.4772.

(48) Yoshioka, K.; Tazawa, E.; Kawai, K.; Enohata, T. Adsorption Characteristics of Superplasticizers on Cement Component Minerals. *Cement and Concrete Research* **2002**, *32* (10), 1507–1513. https://doi.org/10.1016/S0008-8846(02)00782-2.

(49) Khalkhal, F.; Negi, A. S.; Harrison, J.; Stokes, C. D.; Morgan, D. L.; Osuji, C. O. Evaluating the Dispersant Stabilization of Colloidal Suspensions from the

Scaling Behavior of Gel Rheology and Adsorption Measurements. *Langmuir* **2018**, *34* (3), 1092–1099. https://doi.org/10.1021/acs.langmuir.7b03343.

(50) Dalas, F.; Nonat, A.; Pourchet, S.; Mosquet, M.; Rinaldi, D.; Sabio, S. Tailoring the Anionic Function and the Side Chains of Comb-like Superplasticizers to Improve Their Adsorption. *Cement and Concrete Research* **2015**, *67*, 21–30. https://doi.org/10.1016/j.cemconres.2014.07.024.

(51) Lide, D. R. *CRC Handbook of Chemistry and Physics, 85th Edition*; CRC Press, 2004.

(52) Shen, Q.; Zhang, T.; Zhu, M.-F. A Comparison of the Surface Properties of Lignin and Sulfonated Lignins by FTIR Spectroscopy and Wicking Technique. *Colloids and Surfaces A: Physicochemical and Engineering Aspects* **2008**, *320* (1), 57–60. https://doi.org/10.1016/j.colsurfa.2008.01.012.

SUPPLEMENTARY

INFORMATIION

Supporting Information

for

Anomalous variations in the viscous activation energy of suspensions induced by fractal structuring

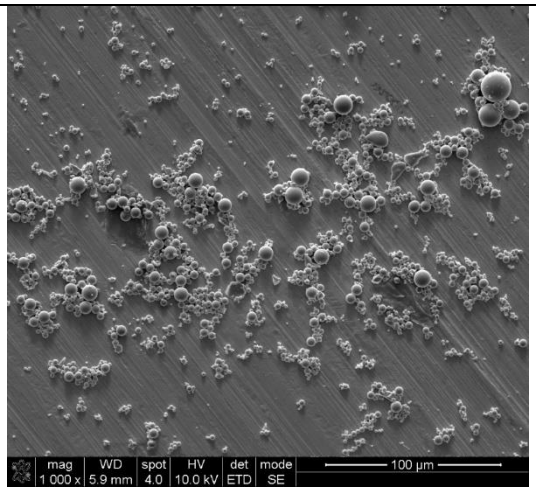

(a)

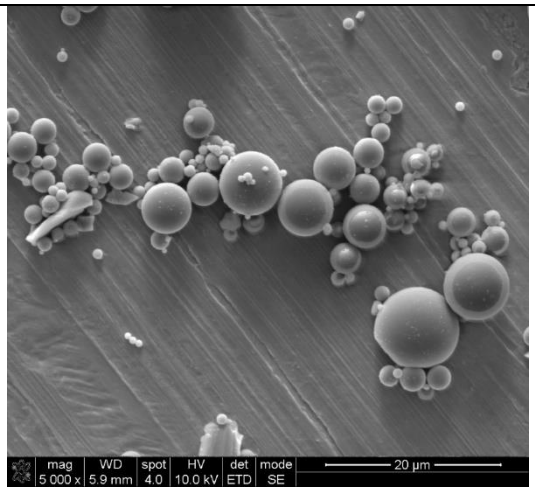

(b)

Figure S1: **(a-b)** SEM images taken of the 5 µm glass beads and used to analyze the shape of the particles. **(b)** was used to count particles and determine their aspect ratio via analysis in ImageJ.

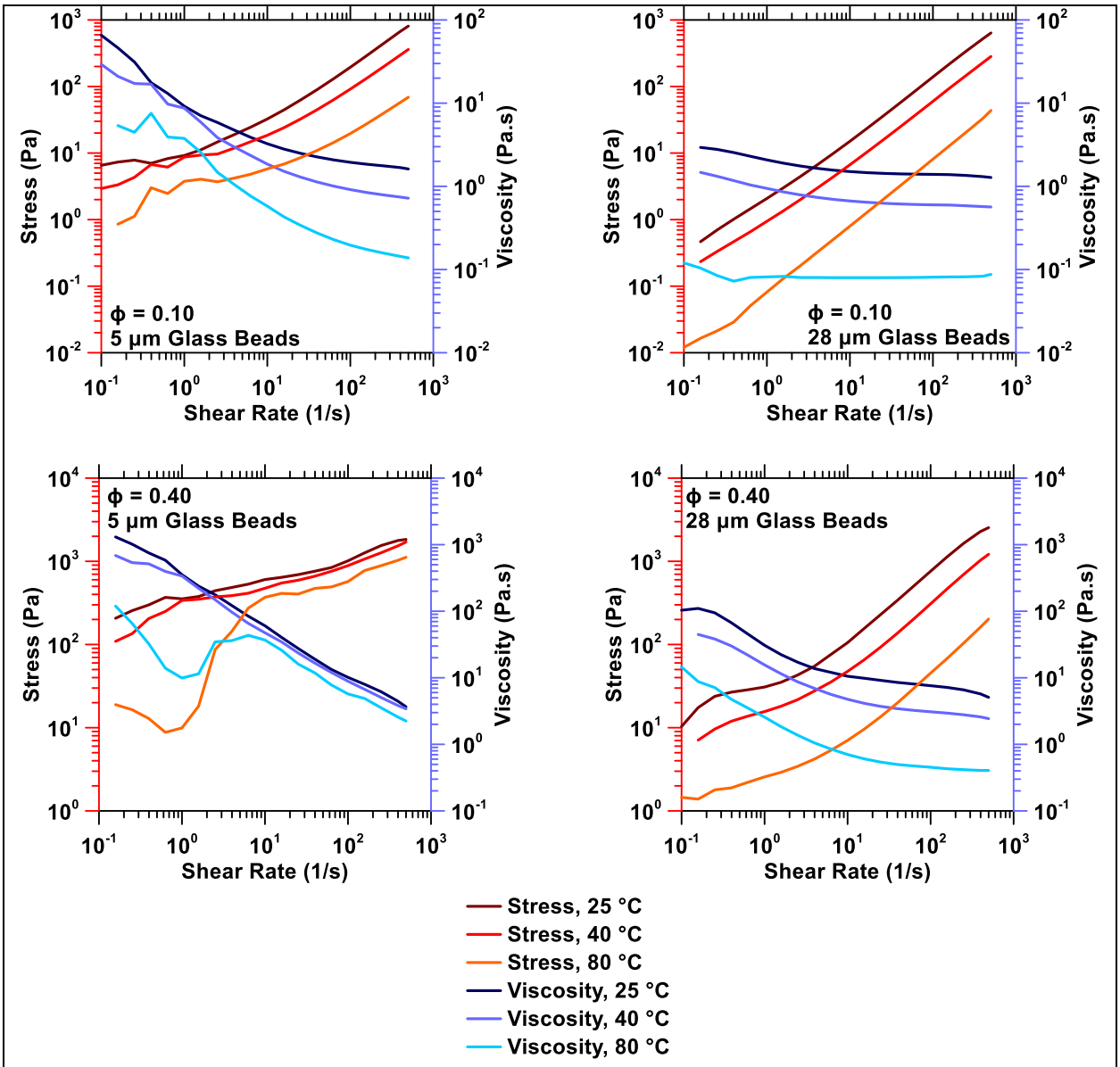

Figure S2: Example viscosity and shear stress data taken directly from the rheometer. Viscosities reported and used for data analysis were taken at a shear rate of 100 1/s.

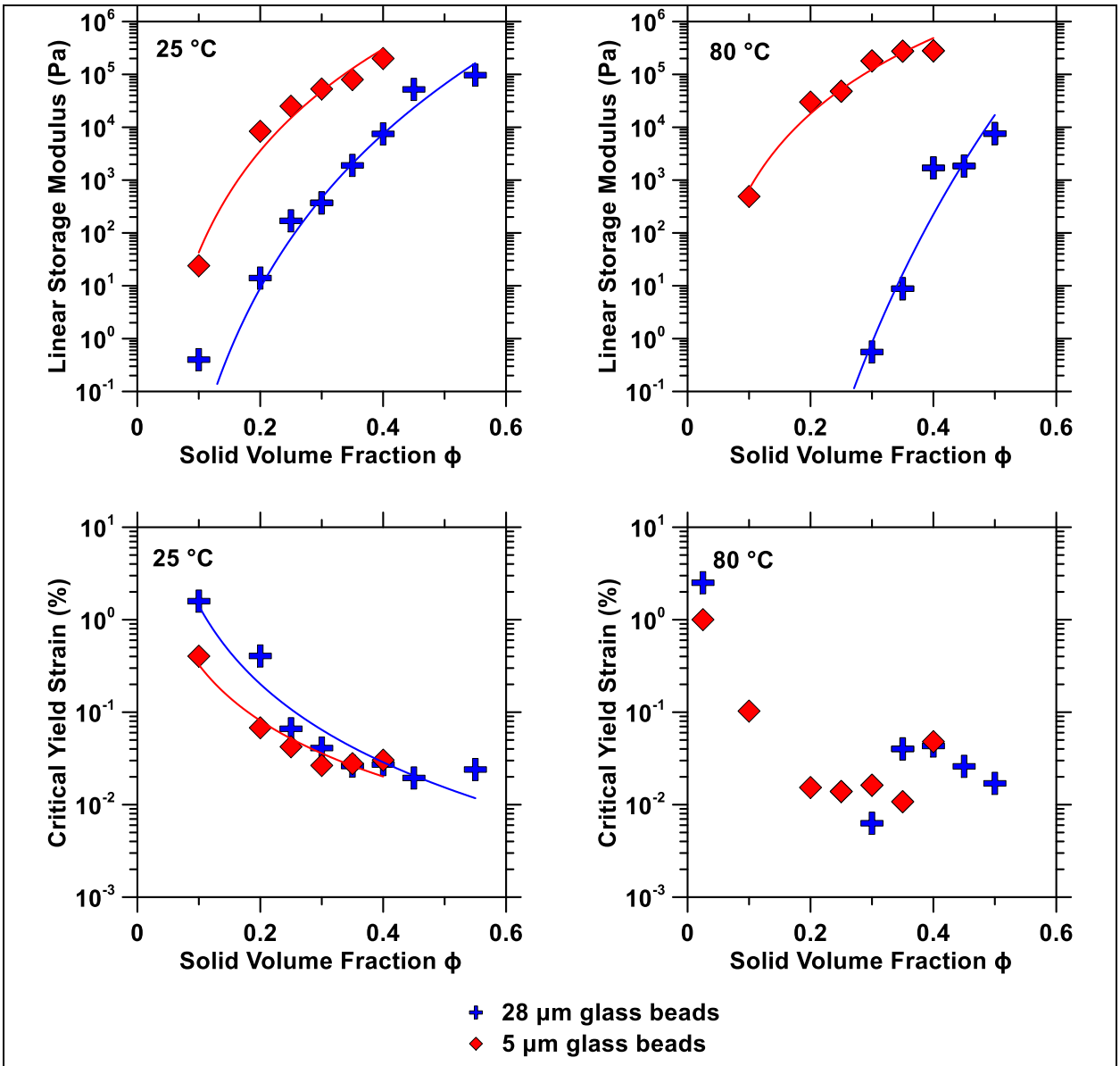

Figure S3: Results for linear storage modulus and critical yield strain for glass bead suspensions at 25 °C and 80 °C. As the calculation of the fractal dimension d_f from these values relied on the use of an additional parameter a, they were not considered for the main body of this paper. All fit lines follow a power law scaling.

Supporting Information

for

Dispersing aggregated suspensions of nanosized calcium hydroxide particles via steric repulsion at high ionic strengths

(A) Fourier Transform Infrared Spectroscopy

Fourier Transform Infrared (FTIR, PerkinElmer Spectrum Two) spectroscopy was performed on each of the three dispersants. From the spectra, shown in Figure S1, three relevant functional groups have been identified: the carbonyl group, present on the PAA backbone, the ether group, present on the side chains in PCE, and the sulfonic acid group, present in LS but also appearing slightly in PAA.

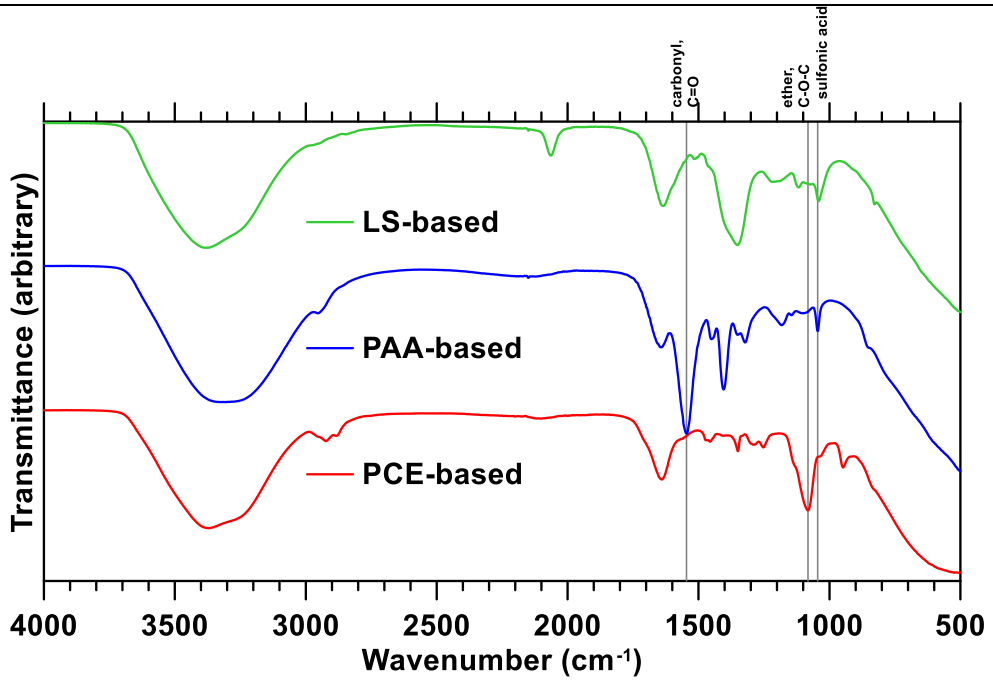

Figure S1: Determination of select functional groups present on each dispersant.

(B) Lifshitz Theory Calculation for Hamaker Constant

The following equation was used to calculate the Hamaker Constant *A* for the suspension of the calcium hydroxide particles (denoted by subscript *p*) and saturated $Ca(OH)_2$ solution (denoted by subscript *m*). It includes terms for the Boltzmann constant (k_b), permittivity (ε), refractive index (n), Planck constant (h), and electron frequency (ν_e).[1]

$$A = \frac{3}{4}kT\left(\frac{\varepsilon_p - \varepsilon_m}{\varepsilon_p + \varepsilon_m}\right)^2 + \frac{3h\nu_e}{16\sqrt{2}}\frac{\left(n_p^2 - n_m^2\right)^2}{\left(n_p^2 + n_m^2\right)^{3/2}}$$	**Equation S1**

(C) Kinetic Stability Criterion

This methodology follows that of Israelachvili.[1]

A suspended particle (mass m_p, diameter D, density ρ_p) have a velocity v due to thermal (Brownian) forces caused by random motion of the solvent, with kinetic energy on the order of the thermal energy, approximately the product of the Boltzmann constant k and the absolute temperature T:

$$\frac{1}{2}m_p v^2 = \frac{1}{2}\left[\frac{4}{3}\pi\left(\frac{D}{2}\right)^3 \rho_p\right]v^2 \approx kT$$	**Equation S2**

The average particle velocity can thus be determined:

$$v \approx \sqrt{\frac{12kT}{\pi d^3 \rho_p}}$$	**Equation S3**

The number density of particles N_p is given by the ratio of the total mass of particles m_{pT} over the mass of a single particle m_p. The total mass of particles can be determined from the particle concentration c and the medium density ρ_m.

$N_p = \frac{m_{pT}}{m_p} = \frac{c\rho_m}{\frac{4}{3}\pi\left(\frac{D}{2}\right)^3 \rho_p}$	**Equation S4**

The cubic root of the number density gives the linear number density of particles, the inverse of which gives the distance between particles – the interparticle spacing *d*.

$d = \frac{1}{\sqrt[3]{N_p}}$	**Equation S5**

Collision frequency f_c is given by the inverse of the time it takes a particle to travel the interparticle distance:

$f_c = \frac{v}{d}$	**Equation S6**

The probability *p* of two particles having sufficient energy to overcome a repulsive barrier *E*:

$p = \exp\left(\frac{-E}{kT}\right)$	**Equation S7**

For a given time *t*, can then determine the minimum barrier for which no collisions are energetic enough to overcome this barrier:

$\left(\frac{E}{kT}\right)_{min} = \ln(tf_c)$	**Equation S8**

This value is dependent on particle size; for 24 hours of stability: 20 nm -> 28 kT, 100 nm -> 25 kT, 200 nm -> 22 kT

(D) Further Yield Stress Results for Suspensions with PCE

The following data in Figure S2 shows further yield stress results determined at a variety of solid volume fraction and PCE dispersant dosages, following the same procedure described in the main body of the paper. It illustrates that the impact of PCE is systematic across the range of yield stresses and solid volume fractions examined here, and that higher solid volume fractions are accessible due to increasing the dosage of PCE.

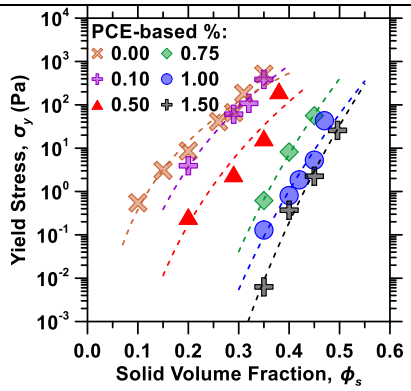

Figure S2: Yield stress-particle volume fraction curves of Ca(OH)2 suspensions at varying PCE dosages. Data was fitted by a power-law function of the form $\sigma_{y,s} = a(\phi)^b$.

(E) Crossover Energy

The crossover energy of some select suspensions at a fixed volume fraction (φ_s = 0.25) was determined. The crossover energy is defined as the integral of the storage modulus (G') from zero strain amplitude (γ) to the crossover point, where the loss modulus (G'') first exceeds the storage modulus. Figure S3a illustrates the method of calculating the crossover energy, and Figure S3b shows the trends with dosage, which follow that of yield stress very closely. The crossover energy is another parameter which describes the strength of aggregates, as it is the energy required

to alter the suspension from a solid-like state (low strain amplitude, high storage modulus) to a liquid-like state (high strain amplitude, $G'' > G'$). Suspensions containing PCE have the lowest crossover energy, signifying that any aggregates present are significantly weaker than those found in suspensions with other dispersants or no dispersant.

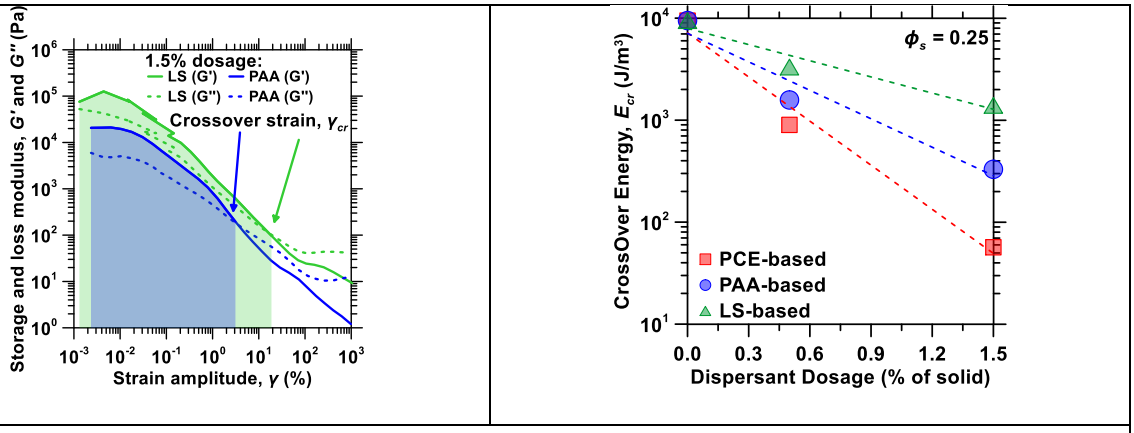

Figure S3: (a) Illustration of the method of calculating crossover energy for two examples of suspensions. **(b)** The dependence of crossover energy of $Ca(OH)_2$ suspensions to dispersant type at varying dispersant dosages.

References

(1) Israelachvili, J. N. *Intermolecular and Surface Forces*; Academic Press, 2015.